Common variants in the lysosomal pathway Contribute to Parkinson's Disease Risk

P. Dimartino[1,2], A. Tenghe[3], S. Khodaee[3], A.A.K. Sreelatha[3], C. Domenighetti[4], P.E. Sugier[4], C. Schulte[5,6], B. Portugal[4], P. May[7], Z. Landoulsi[8], D.R. Bobbili[9], M. Radivojkov-Blagojevic[10], J. Krüger[11], P. Lichtner[10], D.G. Hernandez[12], C. Edsall[12], G.D. Mellick[13], A. Zimprich[14], W. Pirker[15], E. Rogaeva[16], A.E. Lang[17,18,19], S. Koks[20,21], P. Taba[22,23], S. Lesage[24], A. Brice[24], J.C. Corvol[24], M.C. Chartier-Harlin[25], E. Mutez[25], L.G. González Ricardo[3], K. Brockmann[5,6], A.B. Deutschlander[26,27,28], L.F. Burbulla[29,30,31,32], G.M. Hadjigeorgiou[33,34], E. Dardiotis[34], L. Stefanis[35,36], A.M. Simitsi[36], S. Petrucci[37,38], L. Straniero[39,40], R. Asselta[39,40], L. Magistrelli[41], I.U. Isaias[41], A. Zecchinelli[41], G. Pezzoli[42], L. Brighina[43,44], C. Ferrarese[43,44], G. Annesi[45], A. Quattrone[46], M. Gagliardi[47], H. Matsuo[48], A. Nakayama[48], N. Hattori[49], K. Nishioka[49], S.J. Chung[50], Y.J. Kim[51], L. Pavelka[7,8,9,52], I.Y. Bergua[7,9], B.P.C. Van de Warrenburg[53], B.R. Bloem[53], M. Toft[54], L. Pihlstrøm[54], L. Correia Guedes[55,56], J.J. Ferreira[55,57], S. Bardien[58,59], J. Carr[60], A.B. Singleton[12,61], E. Tolosa[62,63], M. Ezquerra[62], P. Pastor[64,65], K. Wirdefeldt[66], N.L. Pedersen[66], C. Ran[67], A.C. Belin[67], A. Puschmann[68], C.E. Clarke[69], K.E. Morrison[70], M. Tan[71], D. Krainc[30], M.J. Farrer[72], A. Elbaz[4], R. Kruger[7,8,9,52], T. Gasser[5,6], E.M. Valente[1,2], M. Sharma[3] on behalf of the COURAGE-PD Consortium

1. Department of Molecular Medicine, University of Pavia, Pavia, Italy
2. Istituto di Ricovero e Cura a Carattere Scientifico (IRCCS) Mondino Foundation, Pavia, Italy
3. Centre for Genetic Epidemiology, Institute for Clinical Epidemiology and Applied Biometry, University of Tübingen, Germany
4. Université Paris-Saclay, UVSQ, Inserm, Gustave Roussy, CESP, 94805, Villejuif, France
5. Department for Neurodegenerative Diseases, Hertie Institute for Clinical Brain Research, University of Tubingen, Germany
6. German Center for Neurodegenerative Diseases (DZNE), Tubingen, Germany
7. Translational Neuroscience, Luxembourg Centre for Systems Biomedicine (LCSB), University of Luxembourg, Esch-Belval, Luxembourg
8. Transversal Translational Medicine, Luxembourg Institute of Health (LIH), Strassen, Luxembourg
9. Luxembourg Centre for Systems Biomedicine (LCSB), University of Luxembourg, Esch-Belval, Luxembourg
10. Institute of Human Genetics, Helmholtz Zentrum München, Neuherberg, Germany
11. Group of Applied Bioinformatics, University of Tübingen, Tübingen, Germany
12. Molecular Genetics Section, Laboratory of Neurogenetics, NIA, NIH, Bethesda, MD 20892, USA
13. Griffith Institute for Drug Discovery, Griffith University, Don Young Road, Nathan, Queensland, Australia
14. Department of Neurology, Medical University of Vienna, Austria
15. Department of Neurology, Klinik Ottakring, Vienna Austria
16. Tanz Centre for Research in Neurodegenerative Diseases, University of Toronto, Toronto, Ontario, Canada
17. Edmond J. Safra Program in Parkinson's Disease, Morton and Gloria Shulman Movement Disorders Clinic, Toronto Western Hospital, UHN, Toronto, Ontario, Canada
18. Division of Neurology, University of Toronto, Toronto, Ontario, Canada
19. Krembil Brain Institute, Toronto, Ontario, Canada

20. Centre for Molecular Medicine and Innovative Therapeutics, Murdoch University, Murdoch, Australia
21. Perron Institute for Neurological and Translational Science, Nedlands, Western Australia, Australia
22. Department of Neurology and Neurosurgery, University of Tartu, Estonia
23. Neurology Clinic, Tartu University Hospital, Tartu, Estonia
24. Sorbonne Université, Institut du Cerveau - Paris Brain Institute - ICM, INSERM, CNRS, Assistance Publique Hôpitaux de Paris, Department of Neurologie, Paris, France
25. University Lille, Inserm, CHU Lille, UMR-S 1172 - JPArc - Centre de Recherche Lille Neurosciences & Cognition, F-59000 Lille, France
26. Department of Neurology, Ludwig Maximilians University of Munich, Germany
27. Department of Neurology, Max Planck Institute of Psychiatry, Munich, Germany
28. Department of Neurology and Department of Clinical Genomics, Mayo Clinic Florida, Jacksonville, FL, USA
29. German Center for Neurodegenerative Diseases (DZNE), Munich, Germany
30. Department of Neurology, Northwestern University Feinberg School of Medicine, Chicago, Illinois 60611, United States
31. Metabolic Biochemistry, Biomedical Center (BMC), Faculty of Medicine, LMU Munich, Munich, Germany
32. Munich Cluster for Systems Neurology (SyNergy), Munich, Germany
33. Department of Neurology, Medical School, University of Cyprus, Nicosia, Cyprus
34. Department of Neurology, Laboratory of Neurogenetics, University of Thessaly, University Hospital of Larissa, Larissa, Greece
35. Center of Clinical Research, Experimental Surgery and Translational Research, Biomedical Research Foundation of the Academy of Athens, Athens, Greece
36. 1st Department of Neurology, Eginition Hospital, Medical School, National and Kapodistrian University of Athens, Athens, Greece
37. Department of Clinical and Molecular Medicine, Sapienza University of Rome, Italy
38. UOC Medical Genetics and Advanced Cell Diagnostics, S. Andrea University Hospital, Rome, Italy
39. Department of Biomedical Sciences, Humanitas University, Pieve Emanuele (Milan), Italy
40. IRCCS Humanitas Research Hospital, Rozzano (Milan), Italy
41. Parkinson Institute, Azienda Socio Sanitaria Territoriale (ASST) Gaetano Pini/CTO, Milano, Italy
42. Fondazione Pezzoli per la Malattia di Parkinson, Milan, Italy
43. Department of Neurology, Fondazione IRCCS San Gerardo dei Tintori, Monza, Italy
44. Department of Medicine and Surgery and Milan Center for Neuroscience, University of Milano Bicocca, Milano, Italy
45. Institute for Biomedical Research and Innovation, National Research Council, Cosenza, Italy
46. Institute of Neurology, Department of Medical and Surgical Sciences, Magna Graecia University, Catanzaro, Italy
47. Department of Medical and Surgical Sciences, Neuroscience Research Center, Magna Graecia University, Catanzaro, Italy
48. Department of Integrative Physiology and Bio-Nano Medicine, National Defense Medical College, Saitama 359-8513, Japan
49. Department of Neurology, Juntendo University School of Medicine, Bunkyo-ku, Tokyo 113-8421, Japan
50. Department of Neurology, Asan Medical Center, University of Ulsan College of Medicine, Seoul, South Korea
51. Department of Neurology, Yonsei University College of Medicine, Seoul, South Korea
52. Parkinson's Research Clinic, Centre Hospitalier de Luxembourg, Luxembourg
53. Radboud University Medical Centre, Donders Institute for Brain, Cognition and Behaviour, Department of Neurology, Nijmegen, The Netherlands
54. Department of Neurology, Oslo University Hospital, Oslo, Norway

55. Instituto de Medicina Molecular João Lobo Antunes, Faculdade de Medicina, Universidade de Lisboa, Lisbon, Portugal
56. Department of Neurosciences and Mental Health, Neurology, Hospital de Santa Maria, Centro Hospitalar Universitario Lisboa Norte (CHULN), Lisbon, Portugal
57. Laboratory of Clinical Pharmacology and Therapeutics, Faculdade de Medicina, Universidade de Lisboa, Lisbon, Portugal
58. Division of Molecular Biology and Human Genetics, Department of Biomedical Sciences, Faculty of Medicine and Health Sciences, Stellenbosch University, Cape Town, South Africa
59. South African Medical Research Council/Stellenbosch University Genomics of Brain Disorders Research Unit, Stellenbosch University, Cape Town, South Africa
60. Division of Neurology, Department of Medicine, Faculty of Medicine and Health Sciences, Stellenbosch University, South Africa
61. Center For Alzheimer's and Related Dementias, NIA, NIH, Bethesda, MD 20892, USA
62. Parkinson's disease & Movement Disorders Unit, Neurology Service, Hospital Clínic de Barcelona, Institut d'Investigacions Biomèdiques August Pi i Sunyer (IDIBAPS), University of Barcelona, Barcelona, Spain
63. Centro de Investigación Biomédica en Red sobre Enfermedades Neurodegenerativas (CIBERNED: CB06/05/0018-ISCIII) Barcelona, Spain
64. Fundació per la Recerca Biomèdica i Social Mútua Terrassa, Terrassa, Barcelona, Spain
65. Movement Disorders Unit, Department of Neurology, Hospital Universitari Mutua de Terrassa, Terrassa, Barcelona, Spain
66. Department of Medical Epidemiology and Biostatistics, Karolinska Institutet, Stockholm, Sweden
67. Centre for Cluster Headache, Department of Neuroscience, Karolinska Institutet, Stockholm, Sweden
68. Lund University, Skåne University Hospital, Department of Clinical Sciences Lund, Neurology, Getingevägen 4, 221 85, Lund, Sweden
69. University of Birmingham and Sandwell and West Birmingham Hospitals NHS Trust, United Kingdom
70. Faculty of Medicine, Health and Life Sciences, Queens University, Belfast, United Kingdom
71. Department of Clinical and Movement Neurosciences, UCL Queen Square Institute of Neurology, University College London, London, UK
72. Department of Neurology, McKnight Brain Institute, University of Florida, Gainesville, FL, USA

*Corresponding author

manu.sharma@uni-tuebingen.de

Supplementary Methods

Single-nucleus RNA-Seq datasets and analytical workflow

Single-nucleus RNA sequencing (snRNA-seq) profiles were obtained from four independent postmortem human cohorts archived in the Gene Expression Omnibus (GEO). The primary dataset (GSE178265), enriched for neuronal nuclei by fluorescence-activated nuclei sorting (FANS), was generated from substantia nigra pars compacta (SNpc) tissue and stratified by NR4A2 expression into NR4A2-positive ($NR4A2^+$) and NR4A2-negative ($NR4A2^-$) fractions [1]. The $NR4A2^+$ fraction was enriched for dopaminergic nuclei, whereas the $NR4A2^-$ fraction represented the complementary non-dopaminergic population. The $NR4A2^+$ subset comprised 42 donors, including 21 controls (4 males, 17 females; mean age 82.0 years, median age 90 years) and 21 PD cases (10 males, 11 females; mean age 80.5 years, median age 82 years) (Supplementary table 13). The $NR4A2^-$ subset comprised 29 donors, including 16 controls (4 males, 12 females; mean age 80.3 years, median age 82 years) and 13 PD cases (9 males, 4 females; mean age 82.0 years, median age 82 years) (Supplementary table 14).

To support cross-region and cross-cohort validation, three additional datasets were incorporated. GSE243639 included SNpc nuclei from 29 postmortem donors: 14 controls (9 males, 5 females; mean age 75.5 years, median age 79 years) and 15 sporadic PD cases (11 males, 4 females; mean age 82.0 years, median age 82 years) [2] (Supplementary table 15). GSE161045 profiled the pericommissural putamen and included four controls (2 males, 2 females; mean age 79.0 years, median age 78.5 years) and four PD cases (2 males, 2 females; mean age 73.0 years, median age 73 years) [3] (Supplementary table 16). GSE157783 comprised midbrain tissue from idiopathic PD cases and matched controls, totaling six controls (5 males, 1 female; mean age 83.0 years, median age 86 years) and five PD cases (4 males, 1 female; mean age 77.4 years, median age 79 years) [4-6] (Supplementary table 17).

All datasets were processed using a unified pipeline in R v4.5.0 with Seurat v5.3.0 [7]. Filtering was performed at the level of individual samples to minimize batch-specific biases. Low-complexity nuclei with fewer than 500 detected RNA counts (nCount_RNA) were excluded. Upper-bound thresholds for transcript counts and detected features (nFeature_RNA) were defined per sample, retaining only nuclei with values below the median plus four standard deviations for each metric. Mitochondrial transcript burden was used as an additional quality criterion, applying dataset-specific cutoffs reported in the original studies (>10% for GSE178265, >2% for GSE243639, and >5% for GSE161045). To reduce artifacts arising from multiplet capture, artificial doublet simulation was performed with Scrublet (version 0.2.3), and nuclei exceeding sample-specific doublet score thresholds — defined by the bimodal distribution of simulated doublet scores — were excluded [8]. After quality control, 98,220 $NR4A2^+$ and 145,376 $NR4A2^-$ nuclei were retained from GSE178265, along with 61,106 nuclei from GSE243639, 17,844 nuclei from GSE161045, and 37,530 nuclei from GSE157783. Counts were normalized using the SCTransform framework, followed by cross-dataset integration with Harmony [9] through Seurat's IntegrateLayers function. Principal component analysis was performed, and neighborhood graphs were constructed using the first 30 principal components.

Unsupervised clustering was performed with the FindClusters algorithm, and low-dimensional embeddings were generated using Uniform Manifold Approximation and Projection (UMAP). Cell identities were assigned by manual curation of canonical marker genes. Non-neuronal populations were defined by AQP4 (astrocytes); CLDN5 and FLT1 (endothelial cells); PDGFRB (pericytes); PLP1 and MOG (oligodendrocytes); PDGFRA and VCAN (oligodendrocyte precursor cells); CSF1R and CX3CR1 (microglia); and THEMIS and CD2 (T lymphocytes). Neuronal populations were identified using RBFOX3 and SYT1 as pan-neuronal markers, with dopaminergic neurons defined by TH,

SLC6A3, SLC18A2, and NR4A2; GABAergic neurons by GAD1, GAD2, and SLC32A1; and glutamatergic neurons by SLC17A6 and SLC17A7.

Differential expressions were evaluated at the cluster level using the Wilcoxon rank-sum test implemented in Seurat's FindMarkers function. Multiple testing correction was performed using the Bonferroni method across all genes tested within each cluster.

Gene expression patterns, differential expression signals, and cross-cohort reproducibility were visualized using heatmaps and dot plots. Heatmaps were used to compare Parkinson's disease (PD) risk gene signatures across harmonized cell populations, displaying log fold-change values from Wilcoxon rank-sum testing. To emphasize robust transcriptional shifts, genes that did not meet significance thresholds (fraction of expressing cells > 0.1 and absolute log fold-change > 0.25) were assigned a value of zero. Combined dot plots were generated to provide an integrated view of gene–cell type relationships across datasets. In these plots, dot diameter reflects the proportion of cells expressing a given gene, and color intensity corresponds to the mean expression level. Statistically significant differential expressions were indicated by a red asterisk, defined as fraction of expressing cells > 0.1, absolute log fold-change > 0.25, and Bonferroni-corrected $P < 0.01$. Graphical rendering and panel assembly were carried out in R using the ggplot2 v4.0.1 and patchwork v1.3.2 packages.

Supplementary Figures

Supplementary Fig. 1: PRS-ice2 C+T barplots (a.) and model fit of PRS calculated at all P-value thresholds (b.) generated during parameter optimisation for the training set best model of the LP-PRS

a.

b.

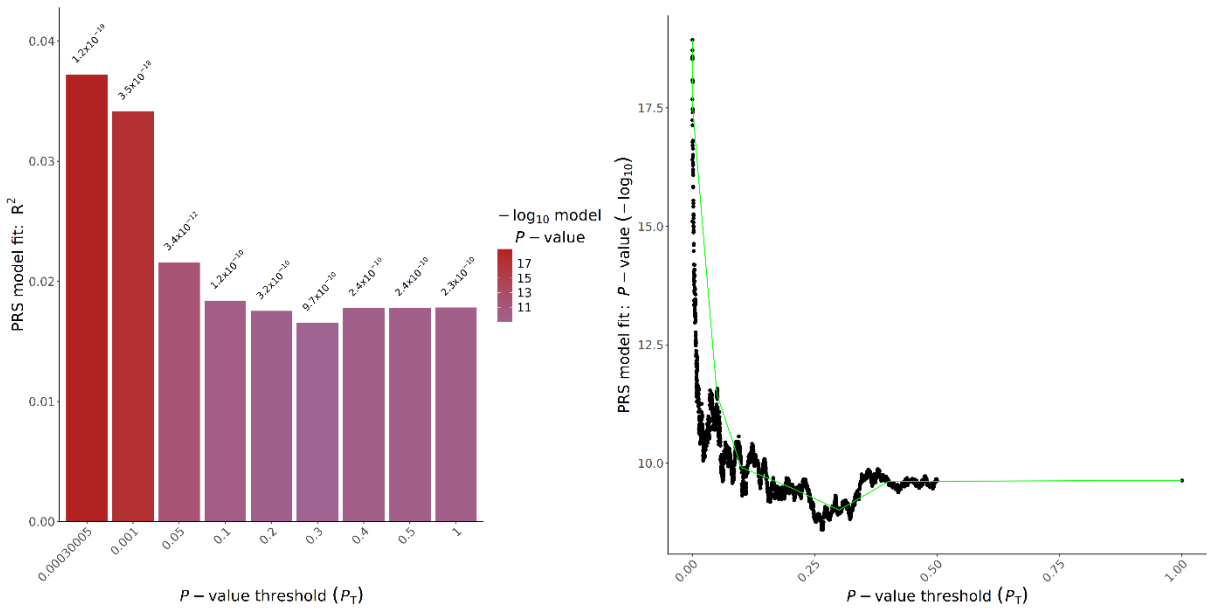

Supplementary Fig. 2: European LP-PRS performances (ROC curves) for the SNP-fixed (a.) and LD-adaptive (b.) models

a.

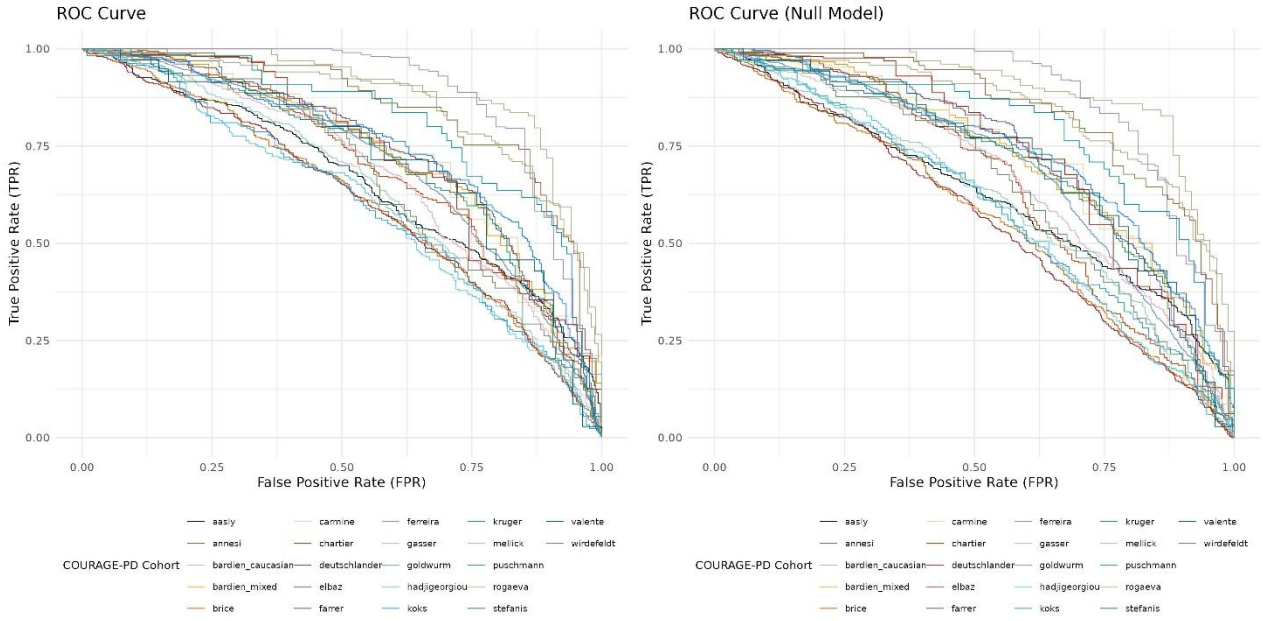

b.

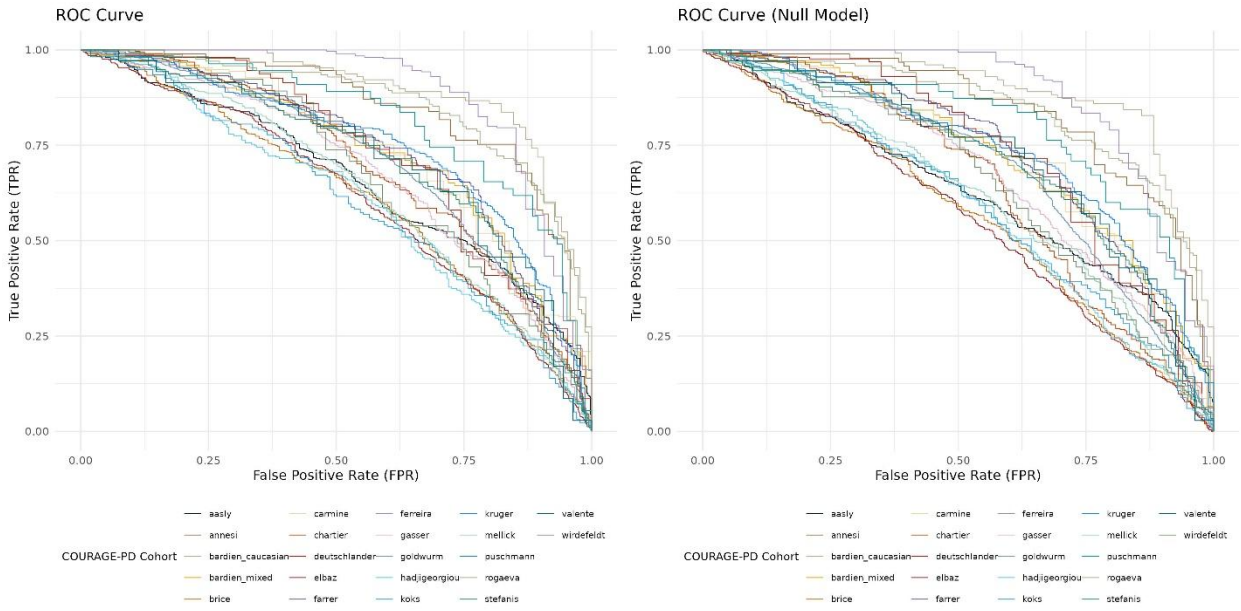

Supplementary Fig. 3: Random-Effect Meta-Analysis in the EUR Cohort

a.

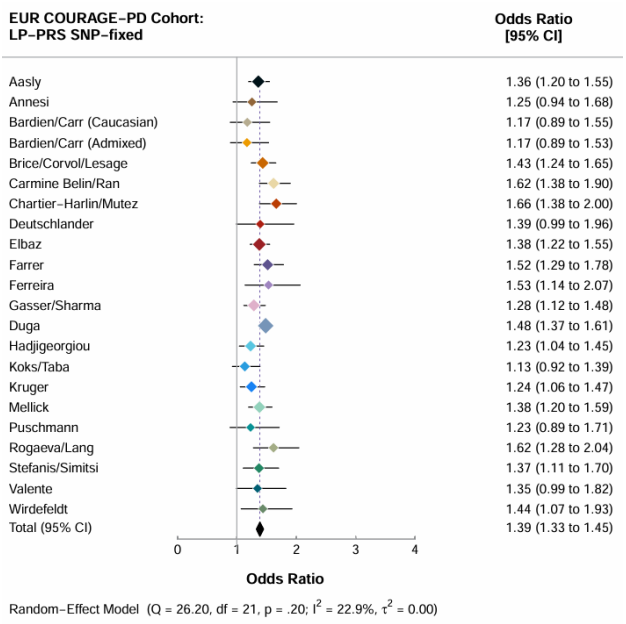

b.

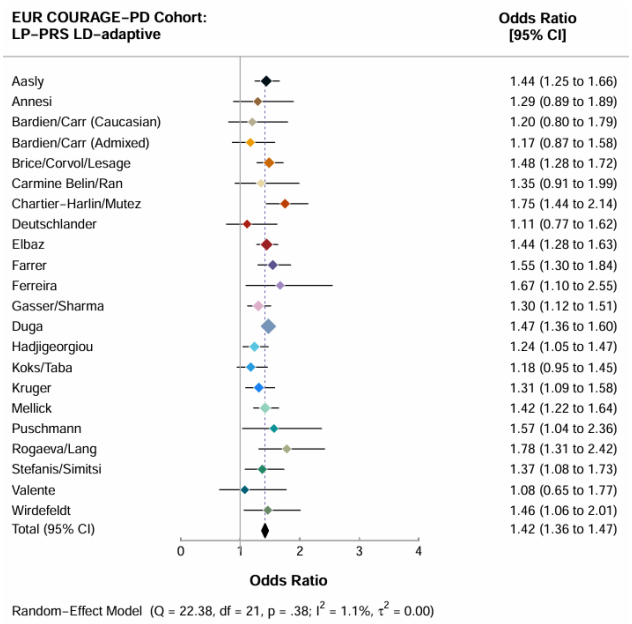

Supplementary Fig. 4: PRS-ice2 C+T barplots (a.) and model fit of PRS calculated at all P-value thresholds (b.) generated during parameter optimisation for the training set best model of the LP-PRS without *LRRK2* and *GBA1*

a.

b.

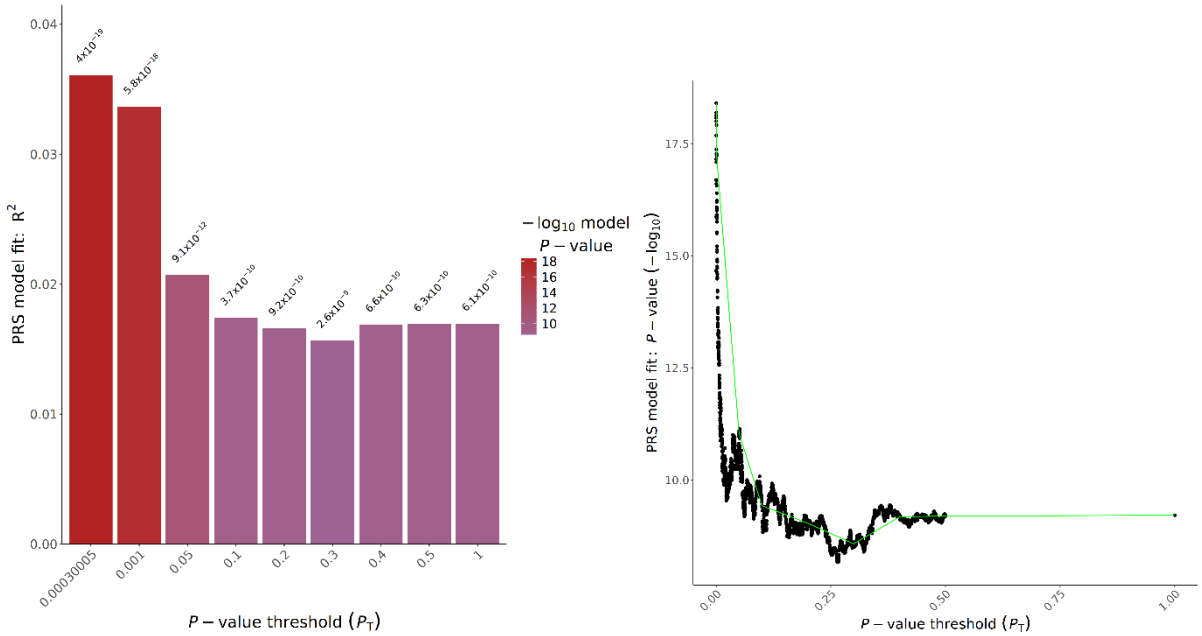

Supplementary Fig. 5: European LP-PRS without LRRK2 and GBA1 performances (ROC curves) for the SNP-fixed (a.) and LD-adaptive (b.) models

a.

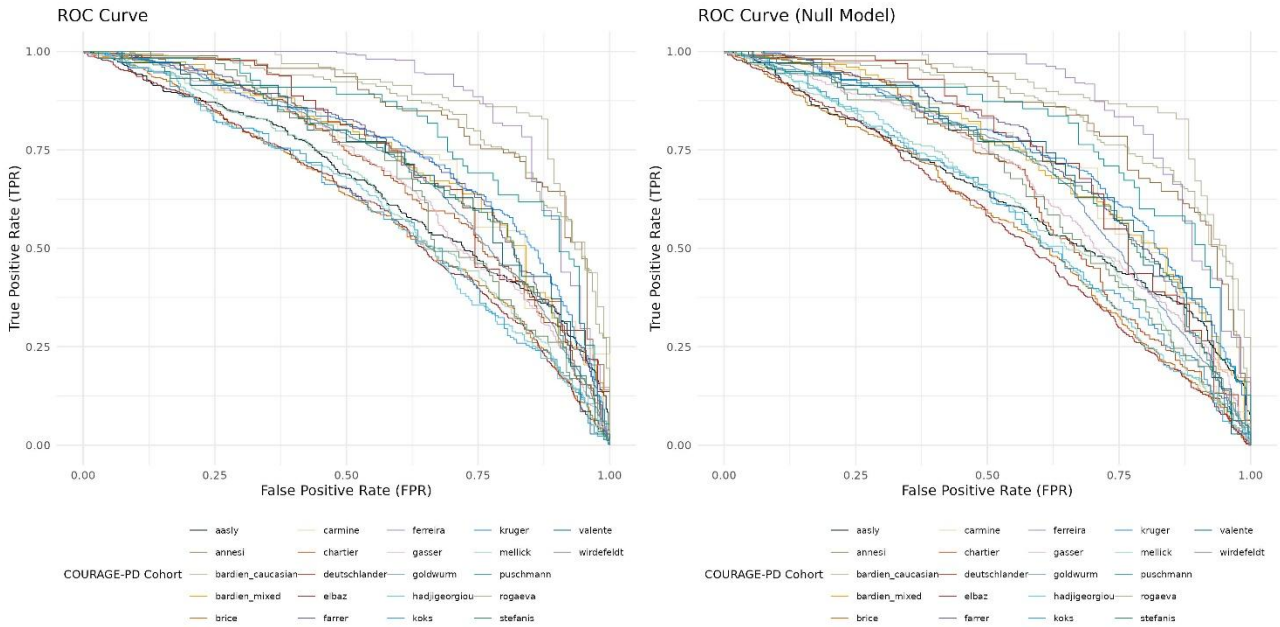

b.

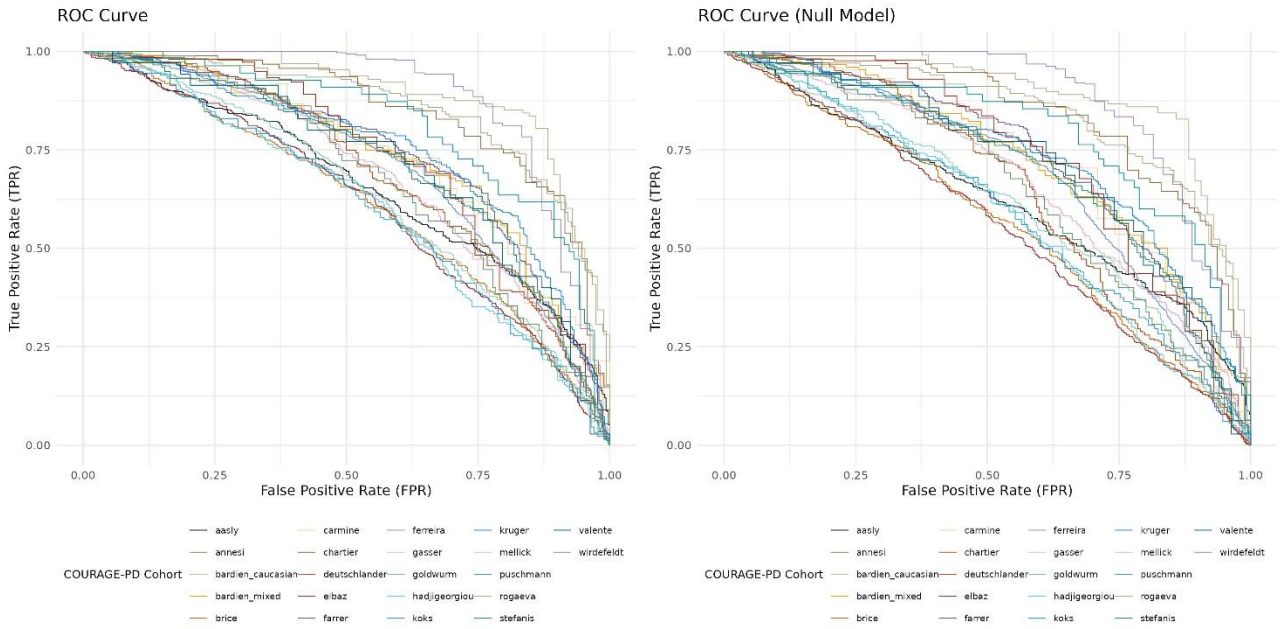

Supplementary Fig. 6: Fixed-Effect Meta-Analysis after excluding SNPs in *LRRK2* and *GBA1*

a.

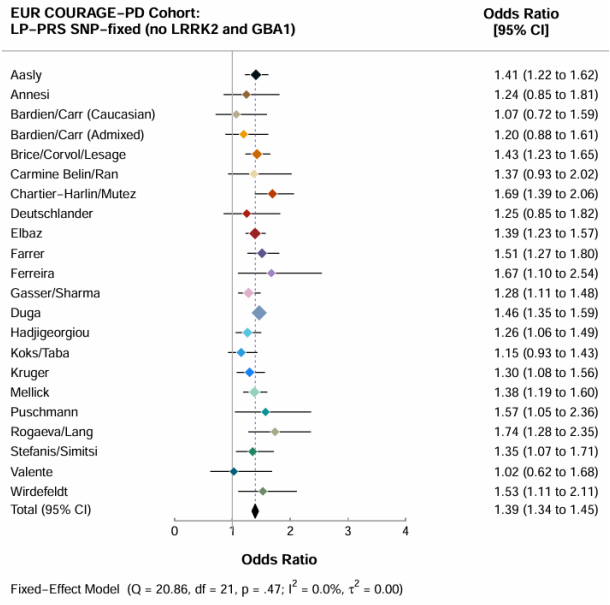

b.

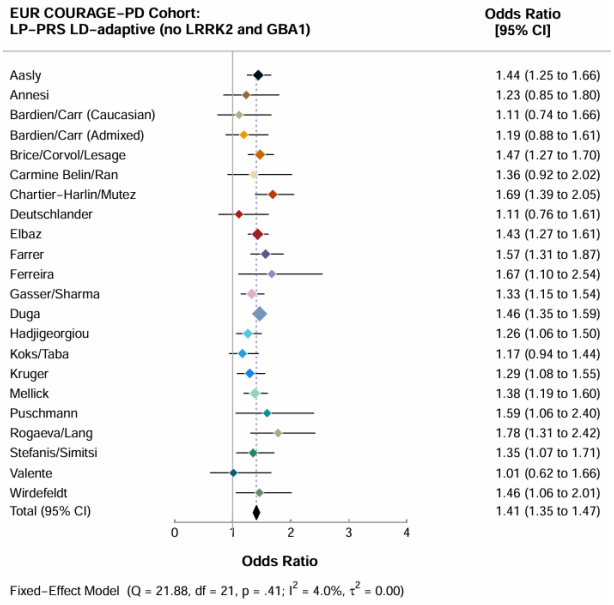

Supplementary Fig. 7: Random-Effect Meta-Analysis after excluding SNPs in *LRRK2* and *GBA1*

a.

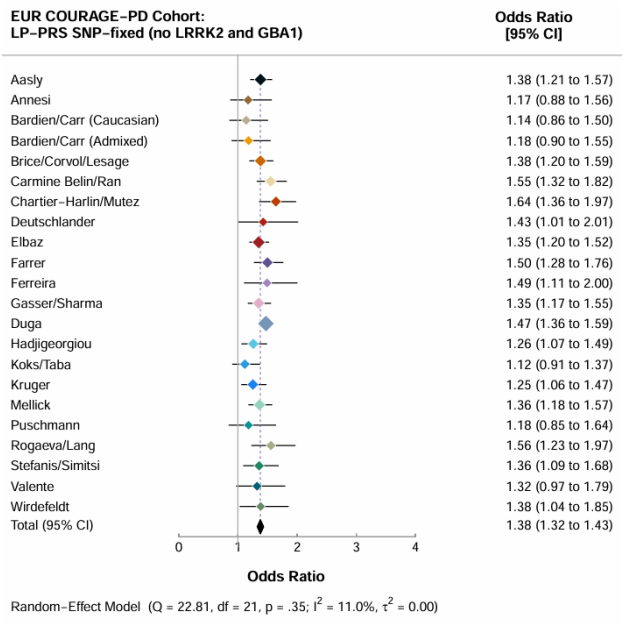

b.

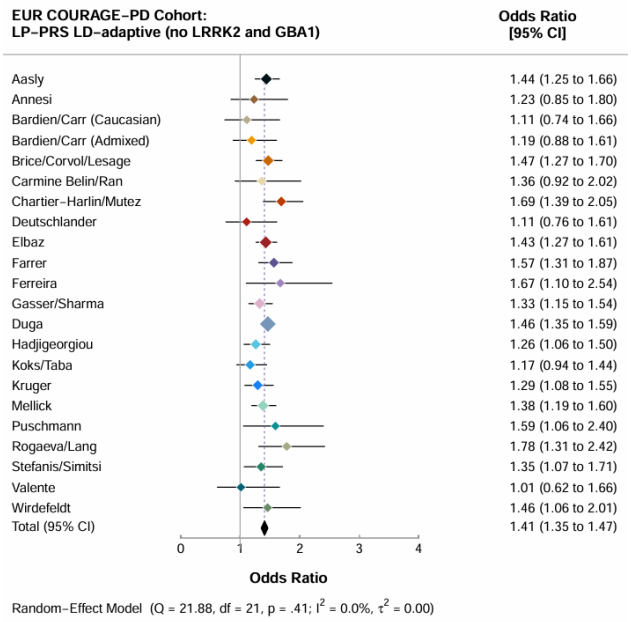

Supplementary Fig. 8: PRS-ice2 C+T barplots (a.) and model fit of PRS calculated at all P-value thresholds (b.) generated during parameter optimisation for the training set best model of the LP-PRS without covariates

a.

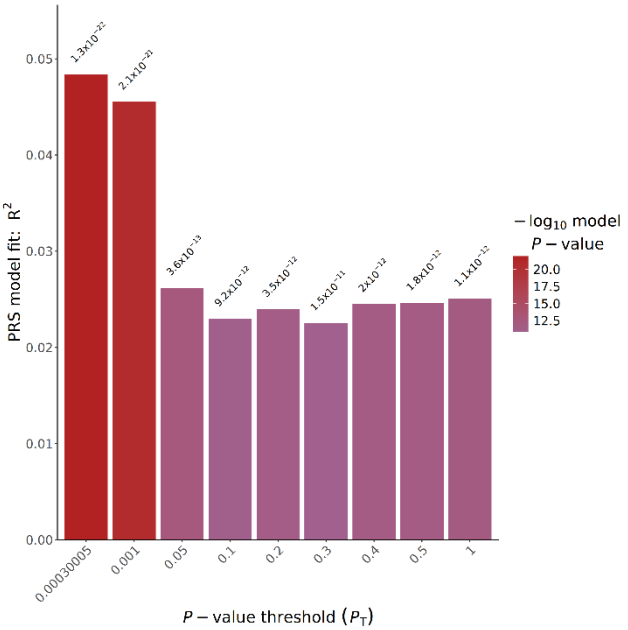

b.

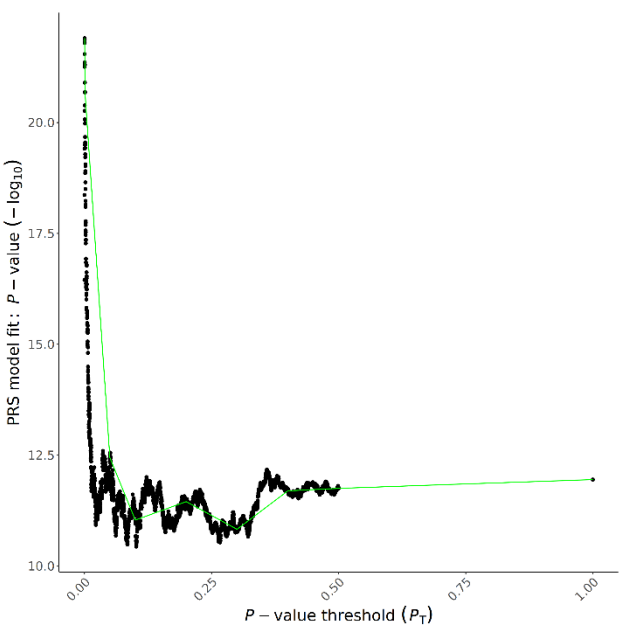

Supplementary Fig. 9: European LP-PRS performances (ROC curves) for the SNP-fixed (a.) and LD-adaptive (b.) models – without covariates

a.

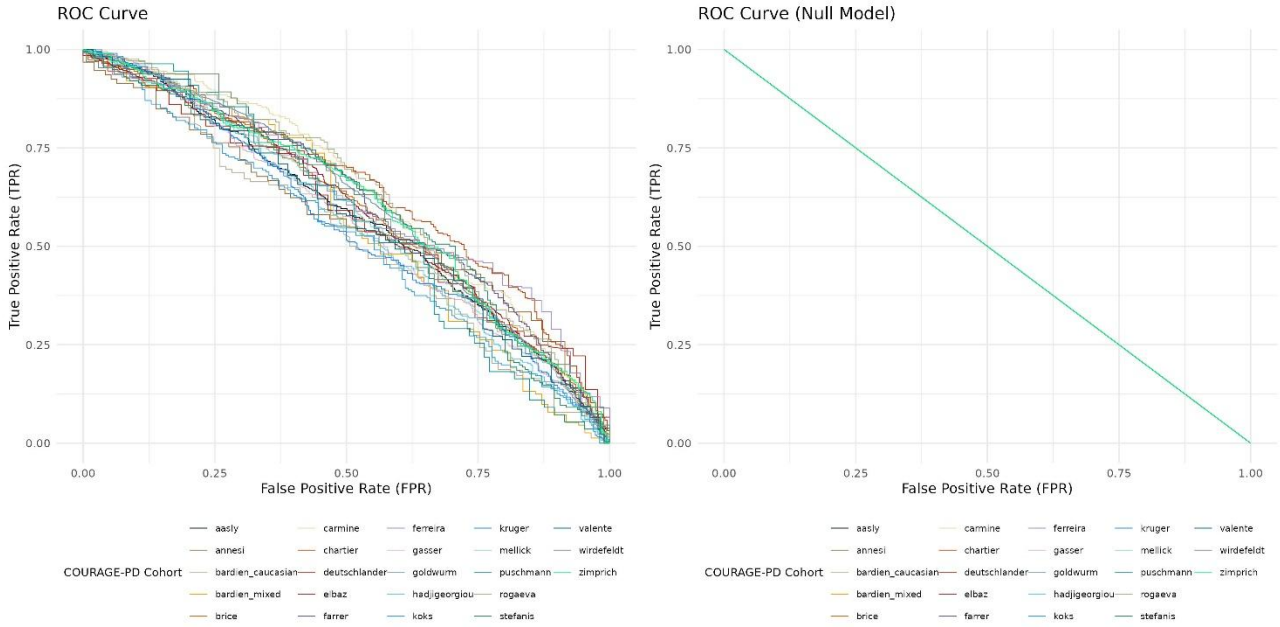

b.

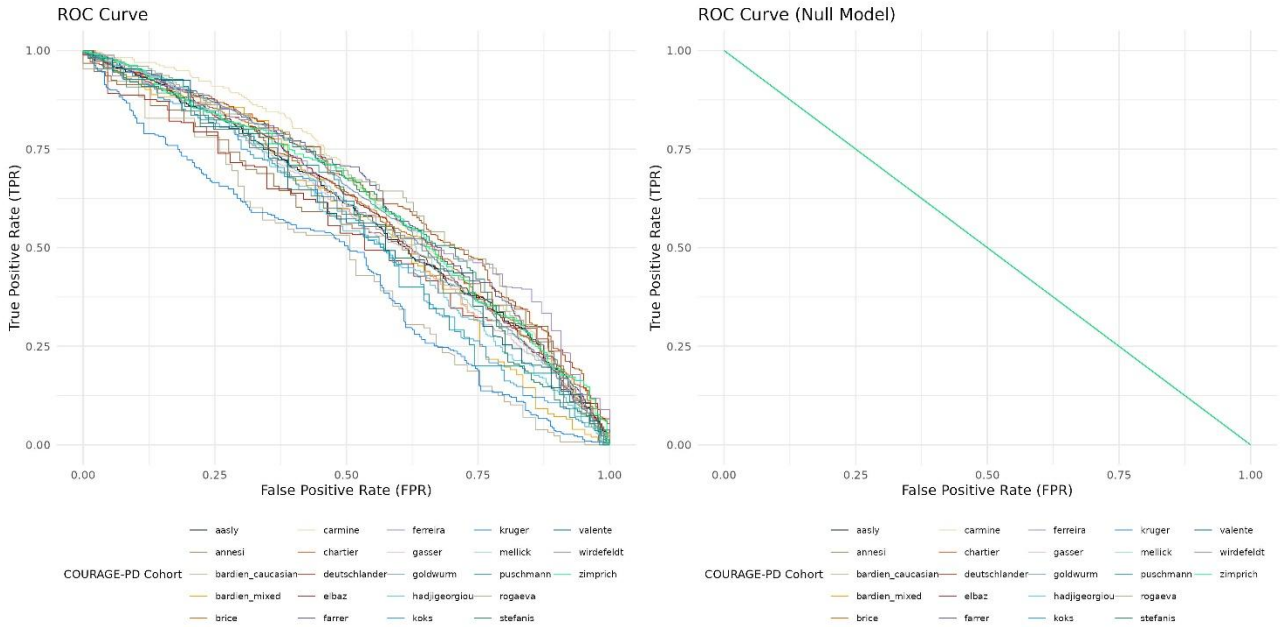

Supplementary Fig. 10: Fixed-Effect Meta-Analysis in the EUR Cohort – without covariates

a.

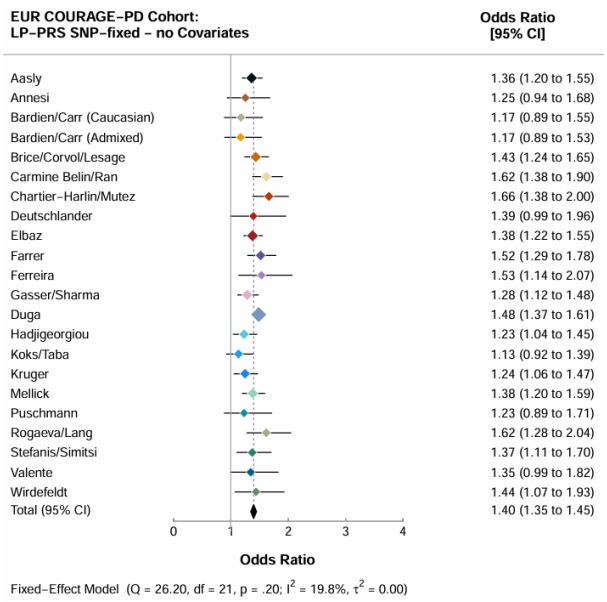

b.

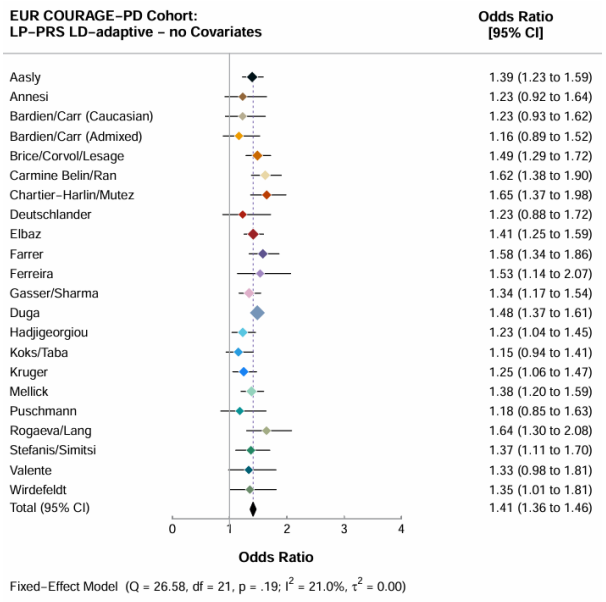

Supplementary Fig. 11: Random-Effect Meta-Analysis in the EUR Cohort – without covariates

a.

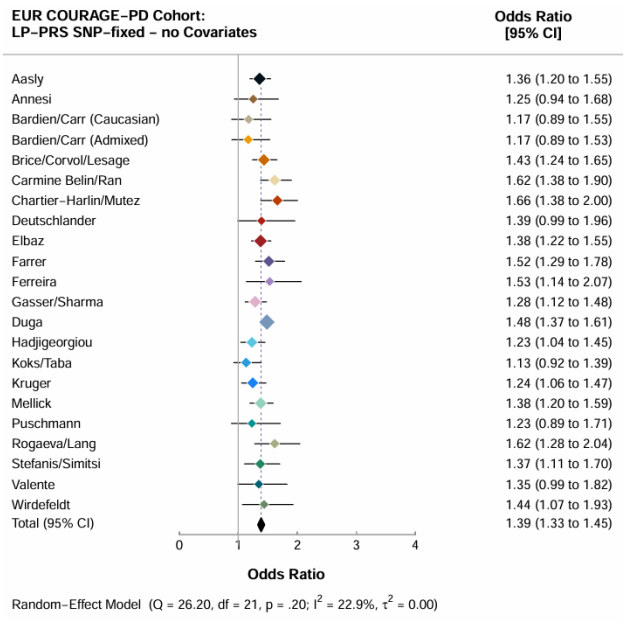

b.

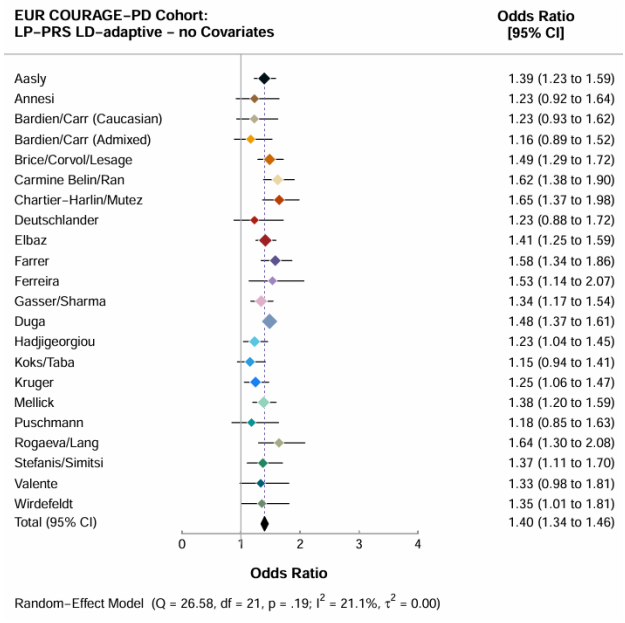

Supplementary Fig. 12: PRS-ice2 C+T barplots (a.) and model fit of PRS calculated at all P-value thresholds (b.) generated during parameter optimisation for the training set best model of the LP-PRS without *LRRK2* and *GBA1* – without covariates

a.

b.

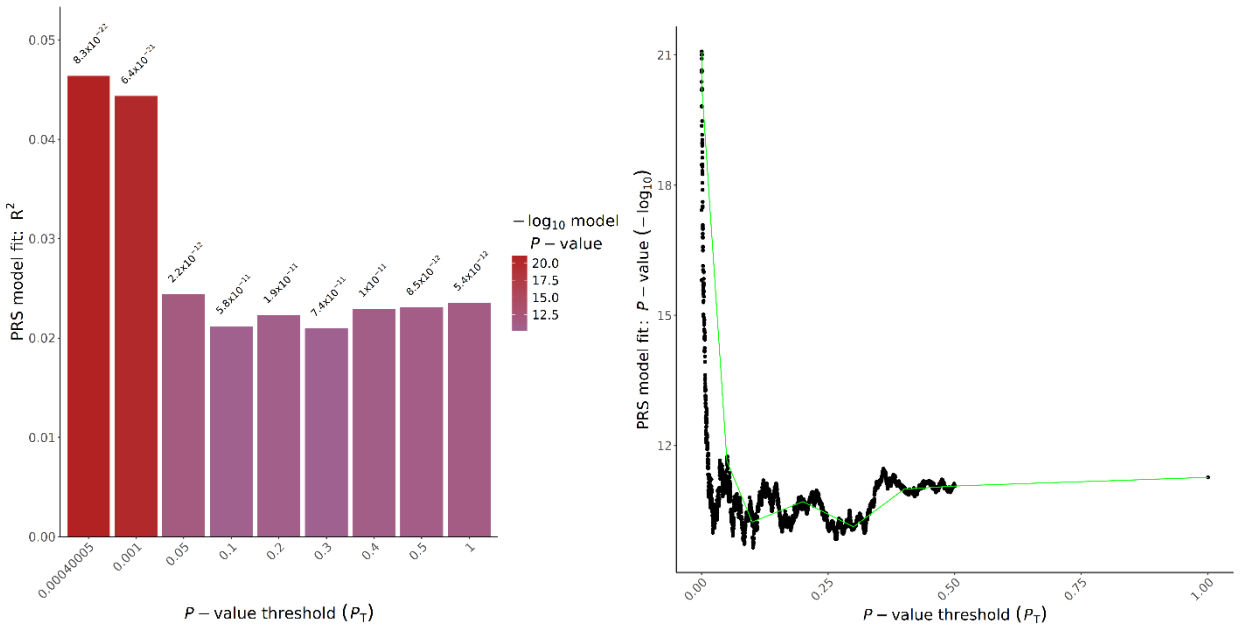

Supplementary Fig. 13: European LP-PRS without LRRK2 and GBA1 performances (ROC curves) for the SNP-fixed (a.) and LD-adaptive (b.) models – without covariates

a.

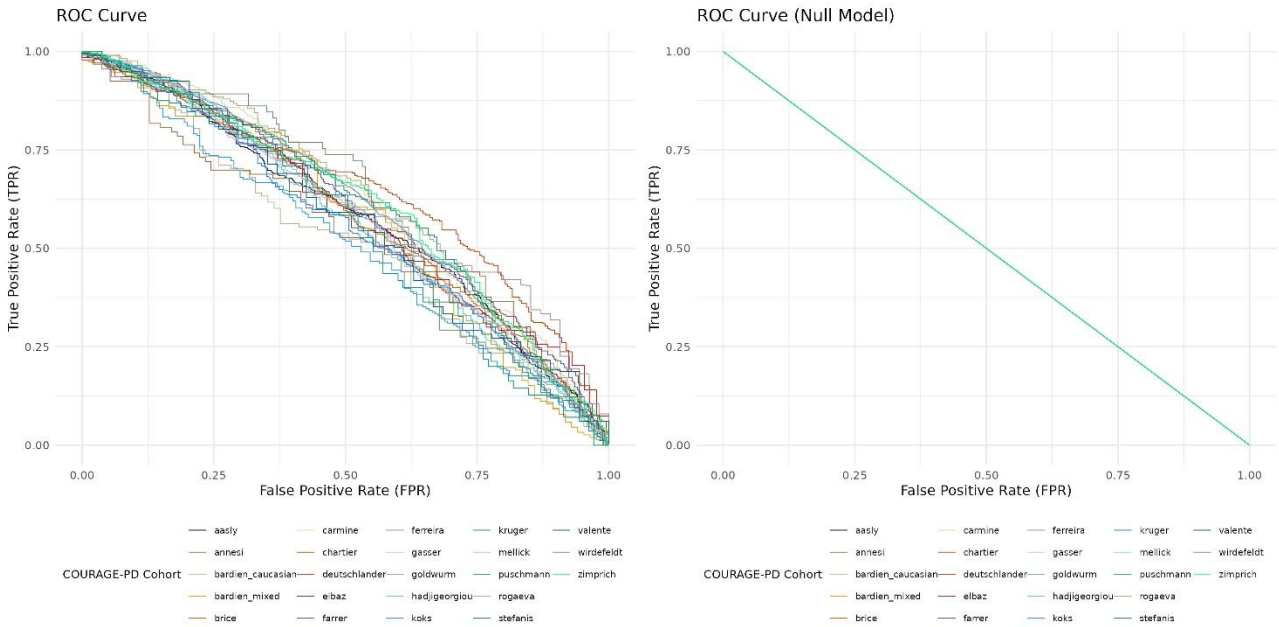

b.

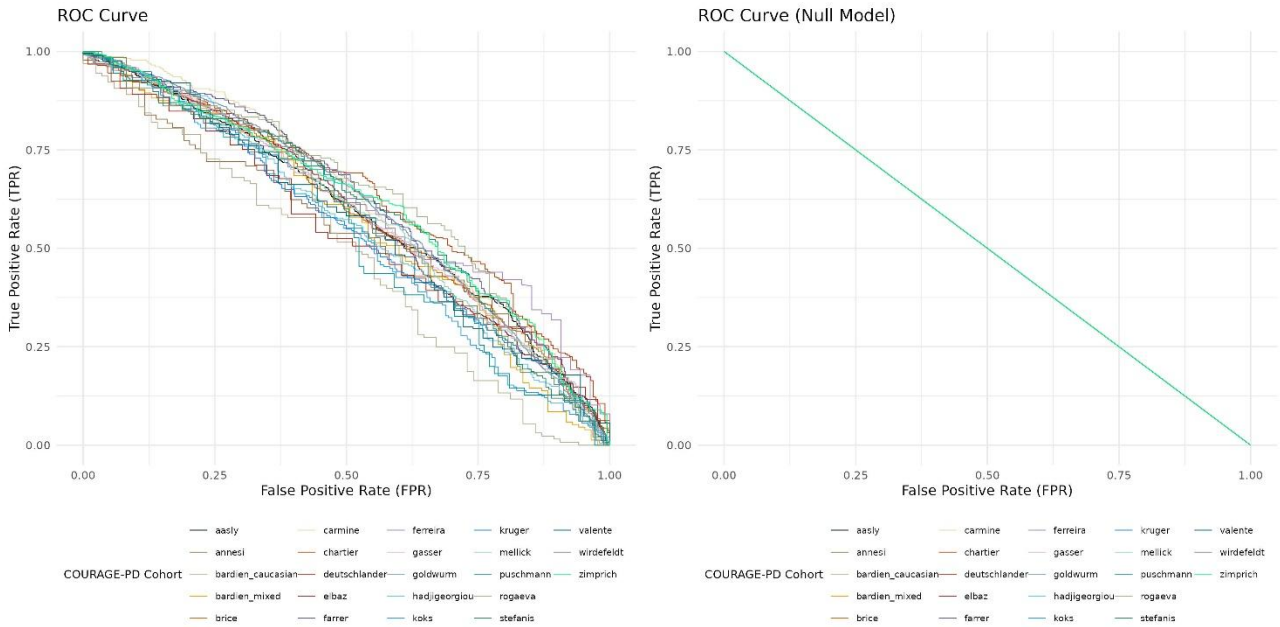

Supplementary Fig. 14: Fixed-Effect Meta-Analysis after excluding SNPs in *LRRK2* and *GBA1* – without covariates

a.

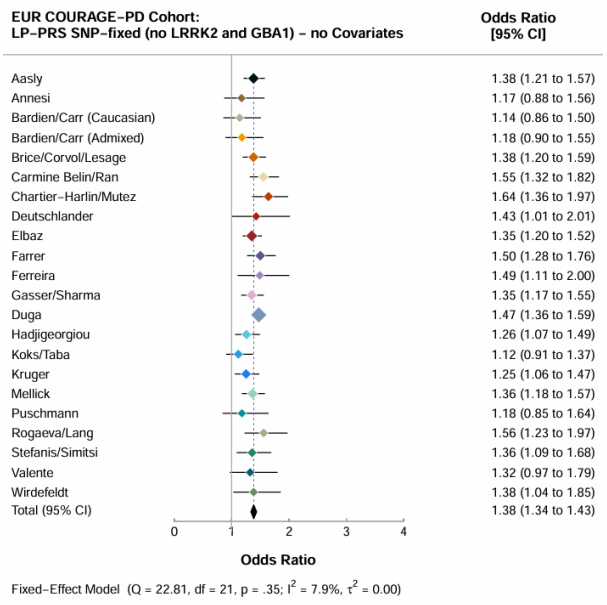

b.

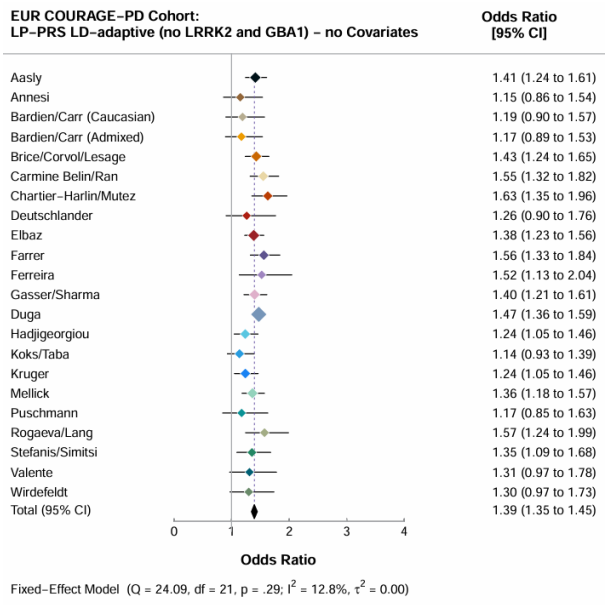

Supplementary Fig. 15: Random-Effect Meta-Analysis after excluding SNPs in *LRRK2* and *GBA1* – no covariates

a.

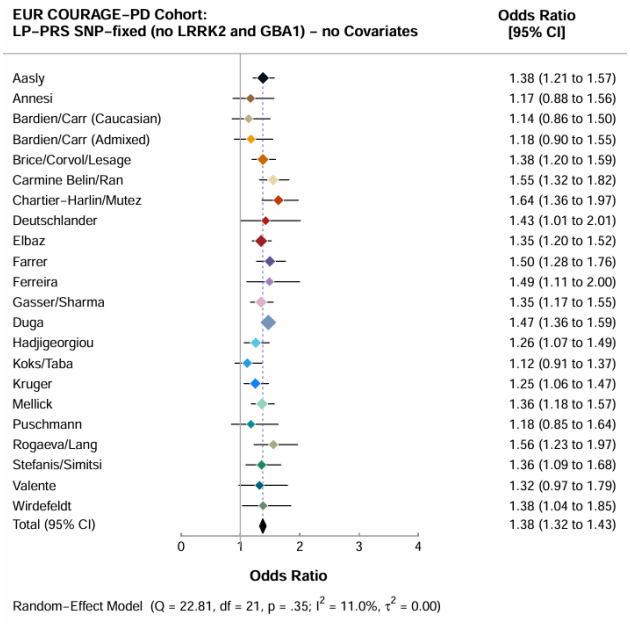

b.

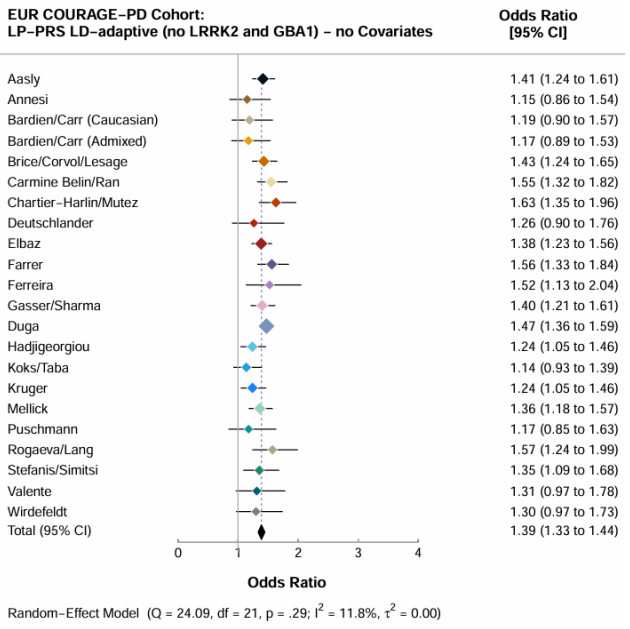

Supplementary Fig. 16: Overall number of SNPs selected with the SNP-fixed and LD-adaptive approaches for the EUR LP-PRS. In bold, the 49 SNPs selected during parameter optimization. Heatmap's color refer to the percentage of the 22 cohorts in which that SNP was used to compute the LD-adaptive LP-PRS

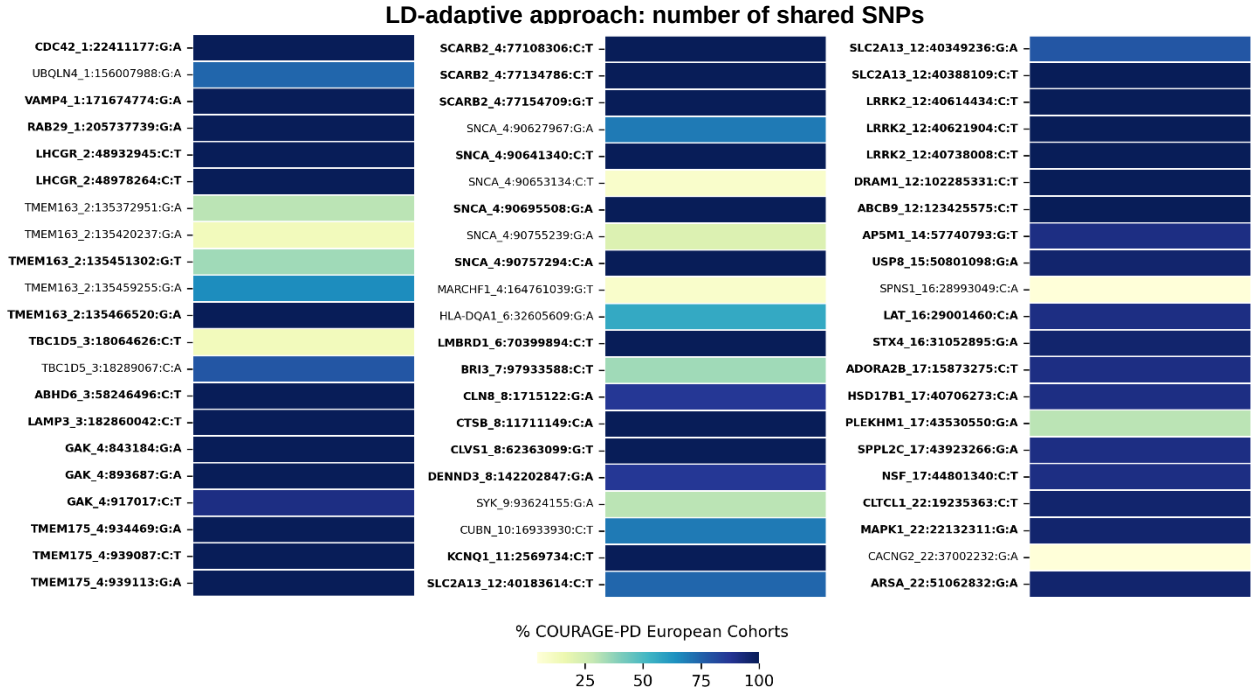

Supplementary Fig. 17: Random-Effect Meta-Analysis in the EAS Cohort

a.

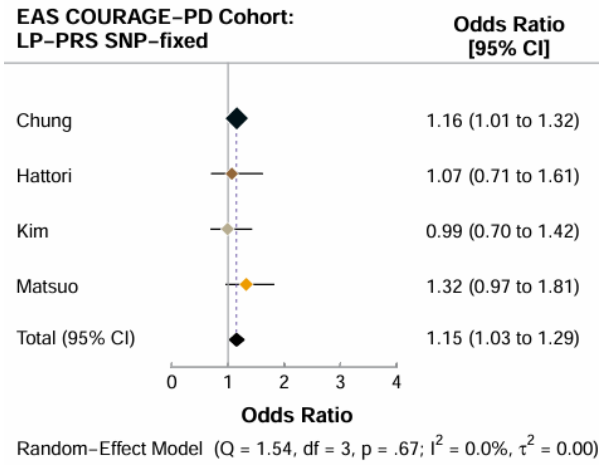

b.

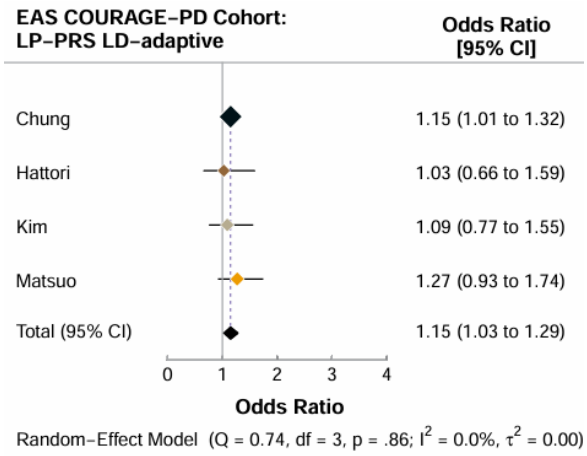

Supplementary Fig. 18: Fixed-Effect Meta-Analysis in the EAS Cohort – without covariates

a.

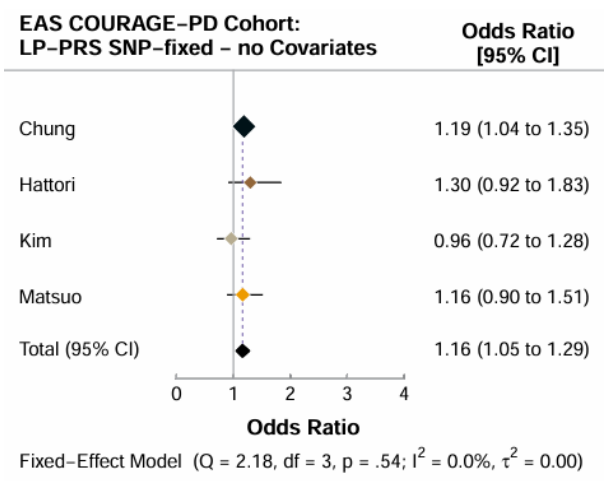

b.

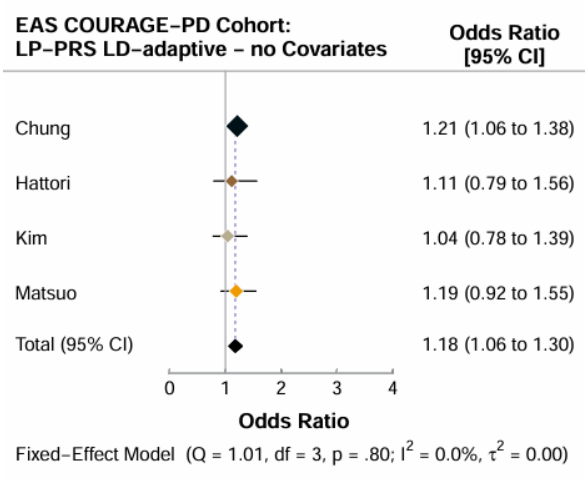

Supplementary Fig. 19: Random-Effect Meta-Analysis in the EAS Cohort – without covariates

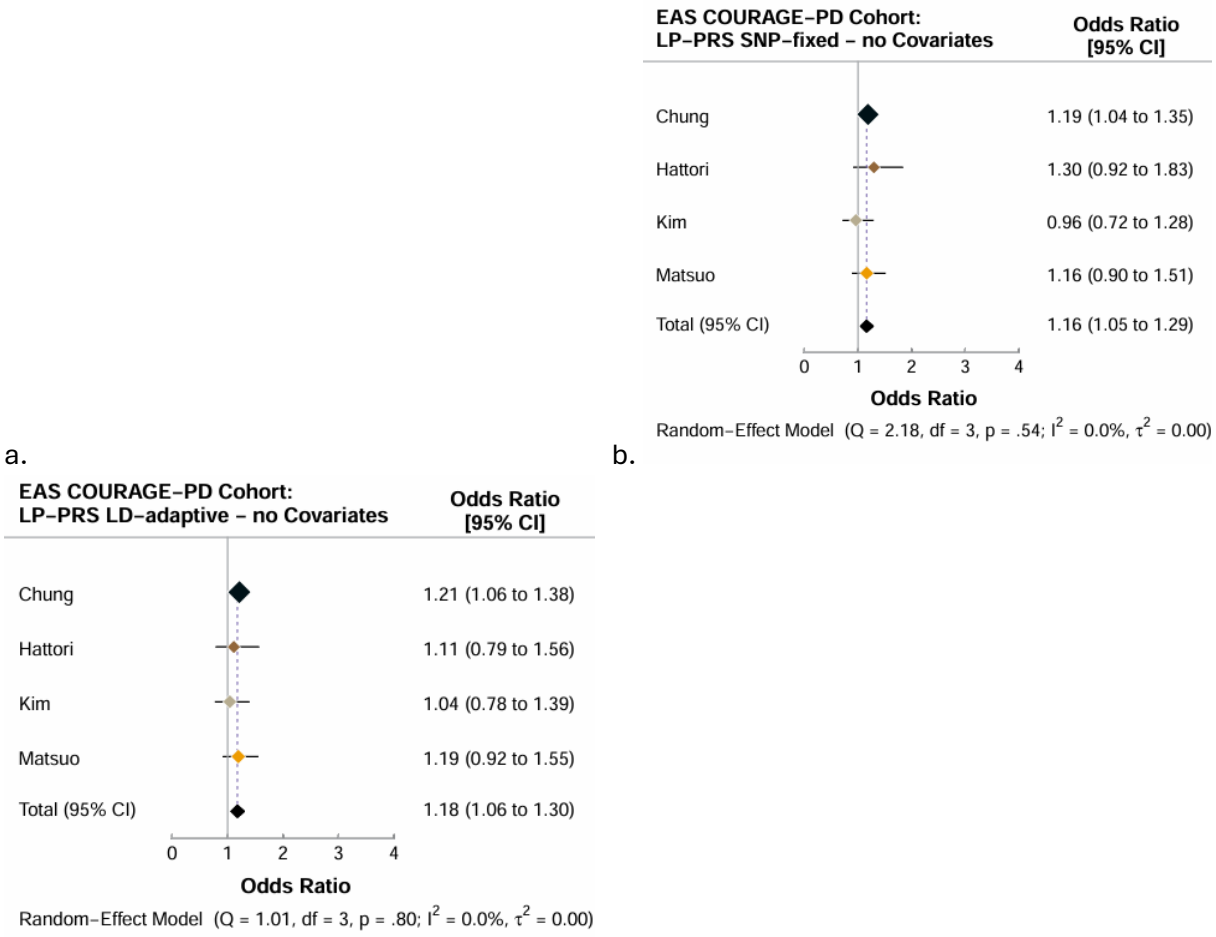

Supplementary Fig. 20: PRS-ice2 C+T barplots (a.) and model fit of PRS calculated at all P-value thresholds (b.) generated during parameter optimisation for the training set best model of the Commander Complex PRS

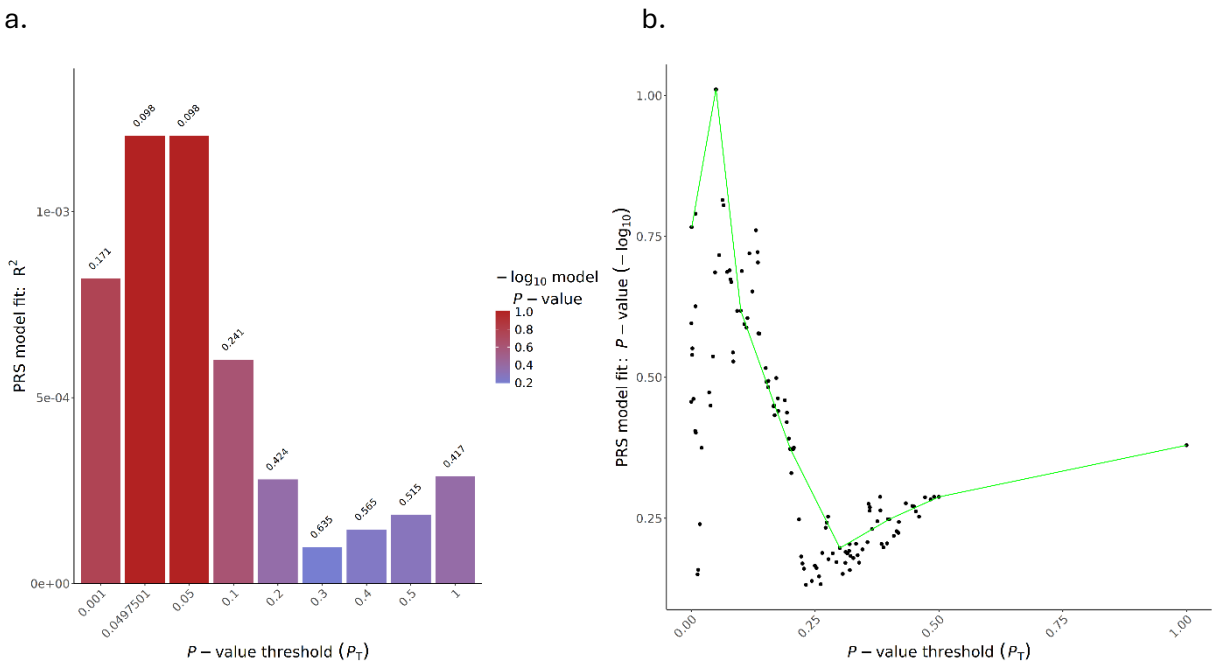

Supplementary Fig. 22: European Commander Complex PRS performances (ROC curves) for the SNP-fixed (a.) and LD-adaptive (b.) models

a.

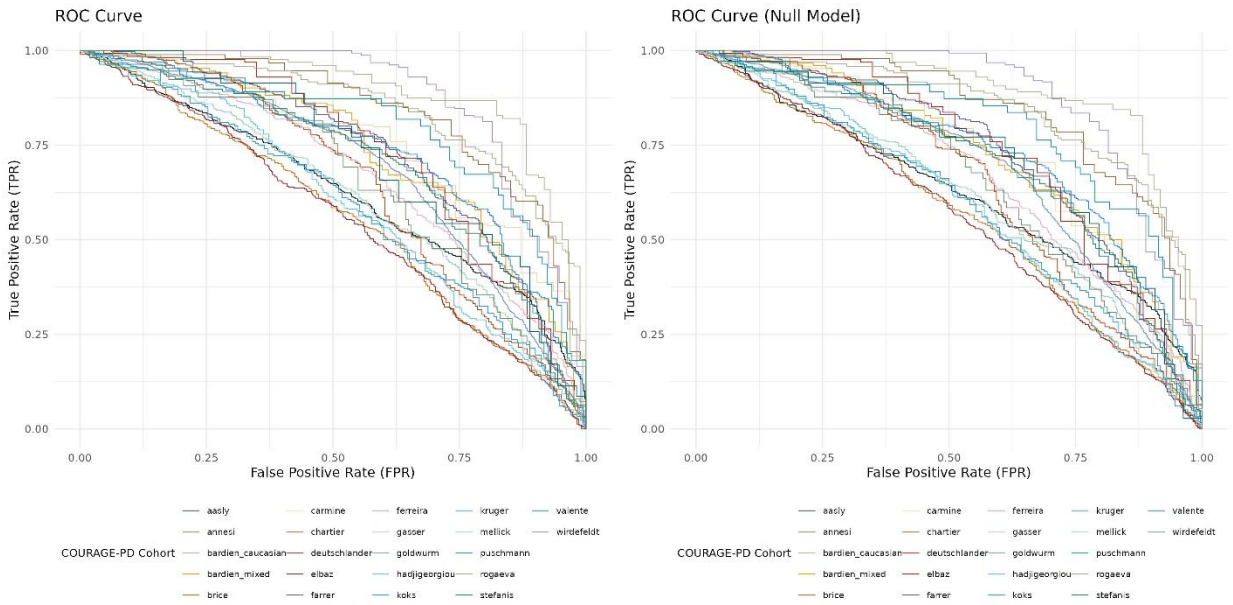

b.

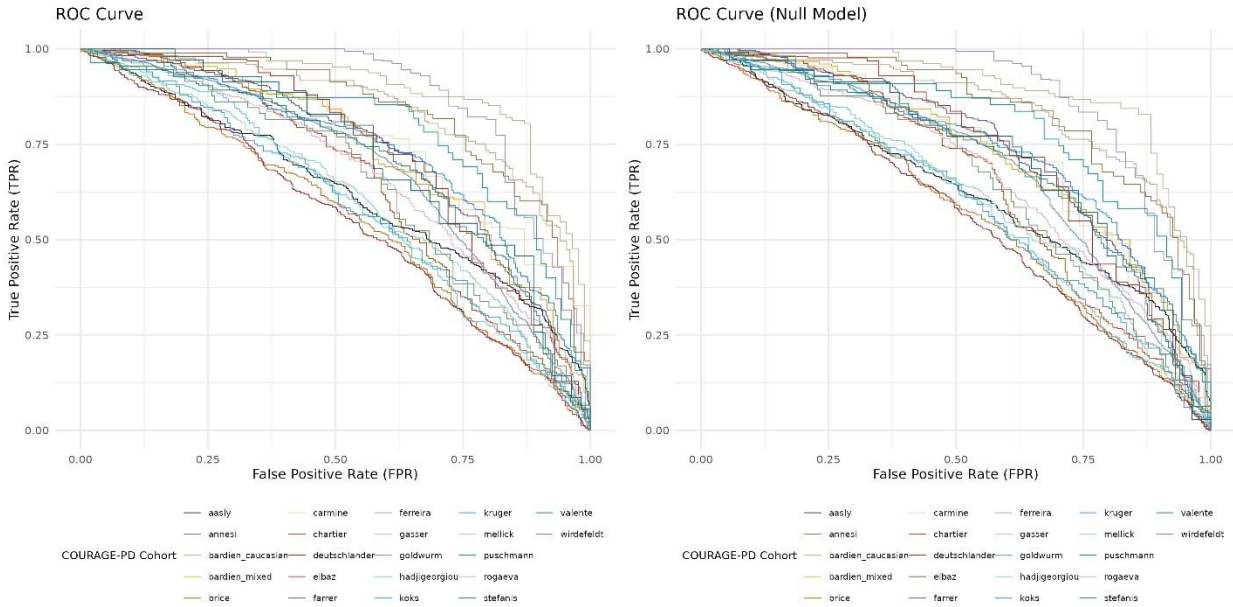

Supplementary Fig. 23: Fixed-Effect Meta-Analysis using SNPs overlapping the Commander Complex genes

a.

b.

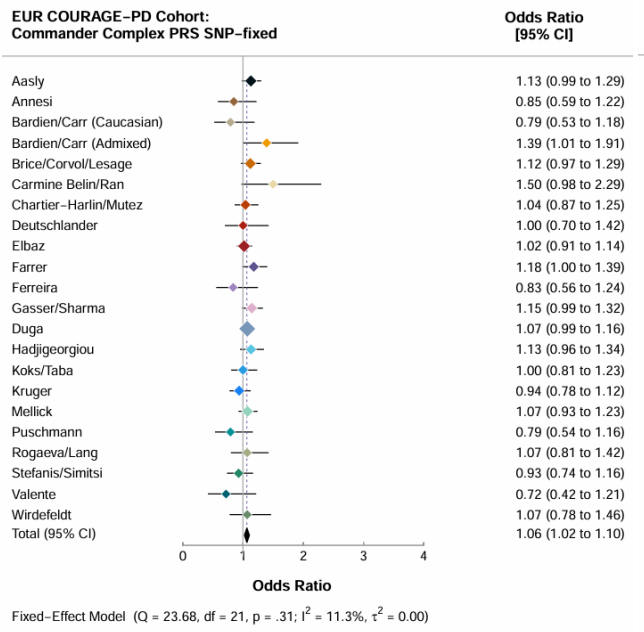

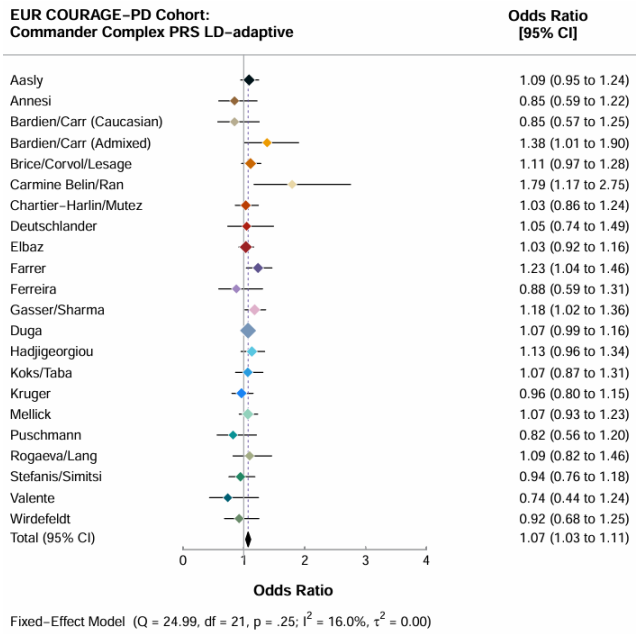

Supplementary Fig. 24: Random-Effect Meta-Analysis using SNPs overlapping the Commander Complex genes

a.

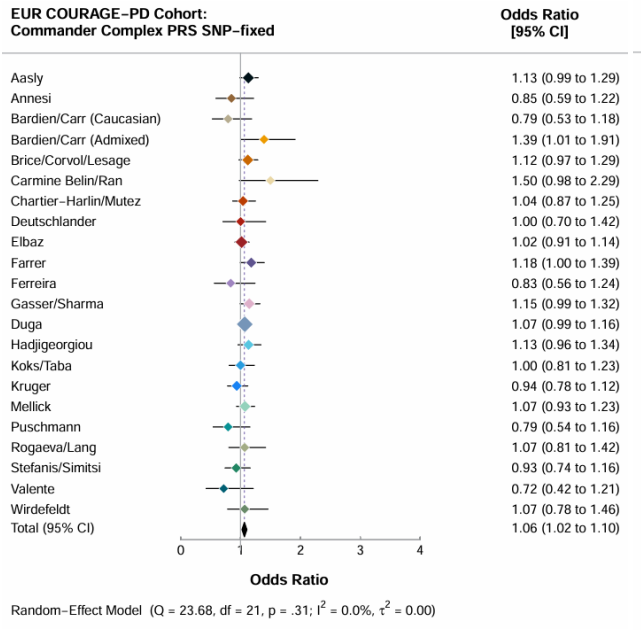

b.

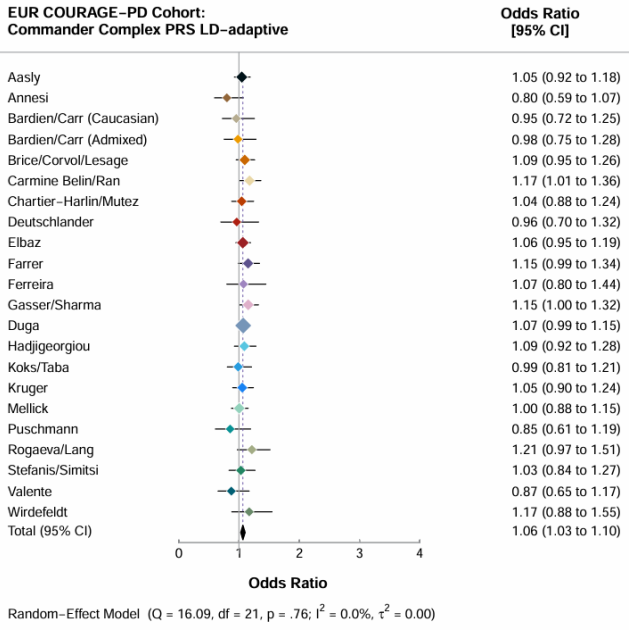

Supplementary Fig. 21: PRS-ice2 C+T barplots (a.) and model fit of PRS calculated at all P-value thresholds (b.) generated during parameter optimisation for the training set best model of the Commander Complex PRS – without covariates

a.

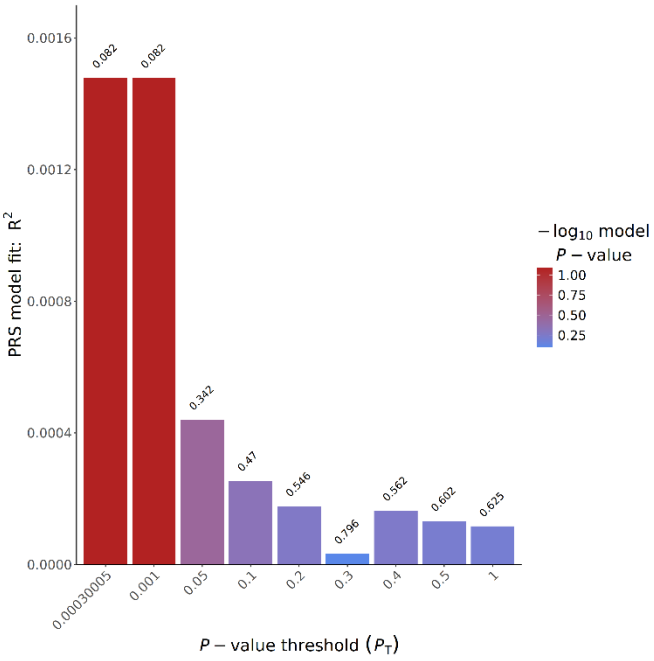

b.

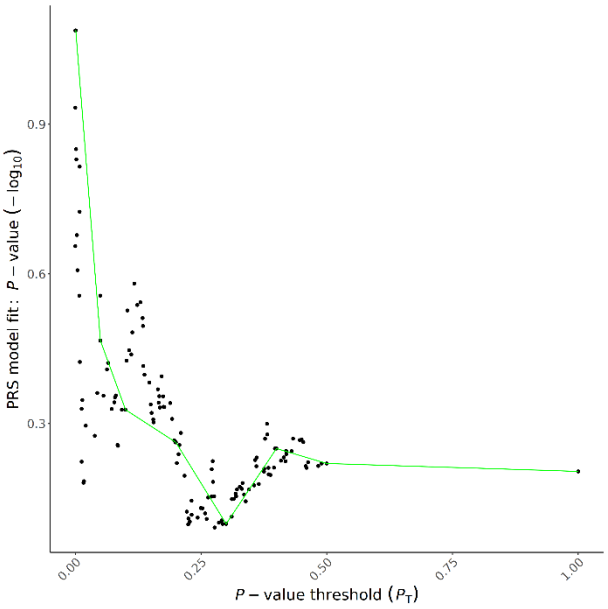

Supplementary Fig. 25: European Commander Complex PRS performances (ROC curves) for the SNP-fixed (a.) and LD-adaptive (b.) models – without covariates

a.

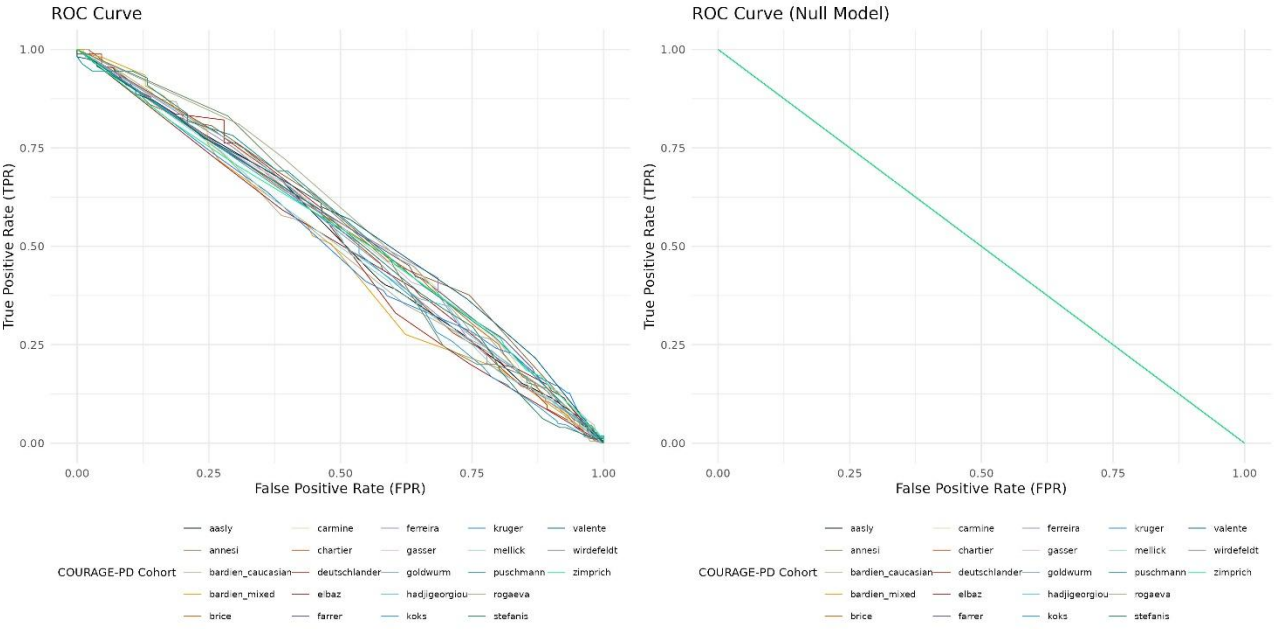

b.

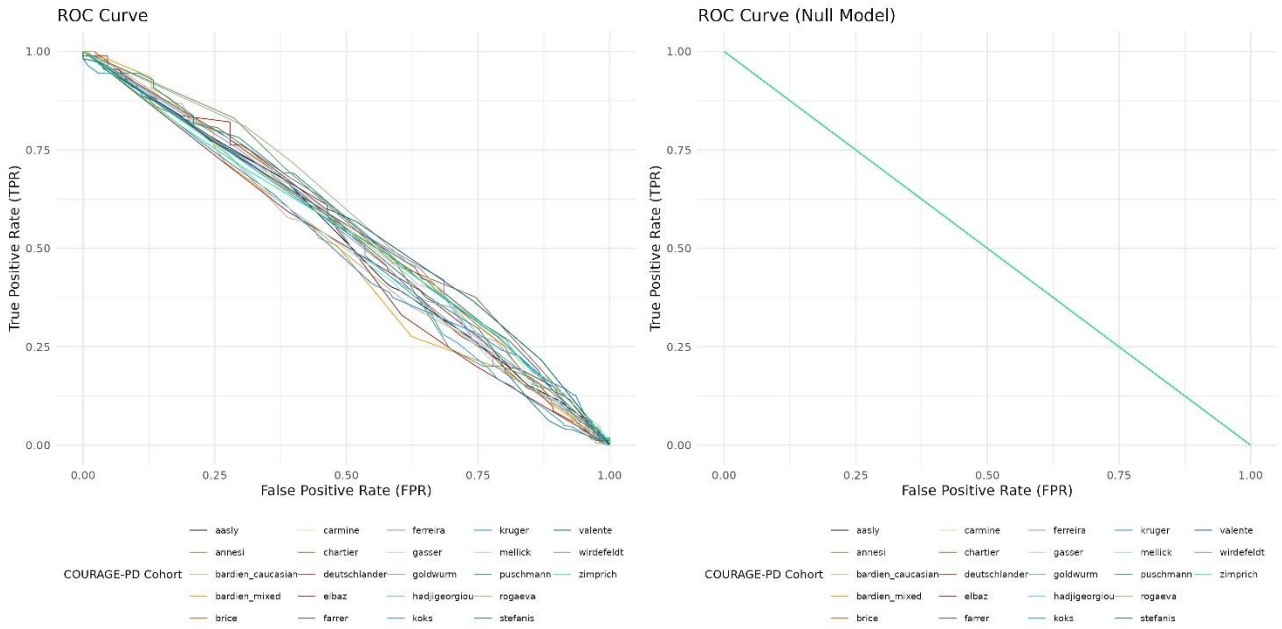

Supplementary Fig. 26: Fixed-Effect Meta-Analysis using SNPs overlapping the Commander Complex genes – no covariates

a.

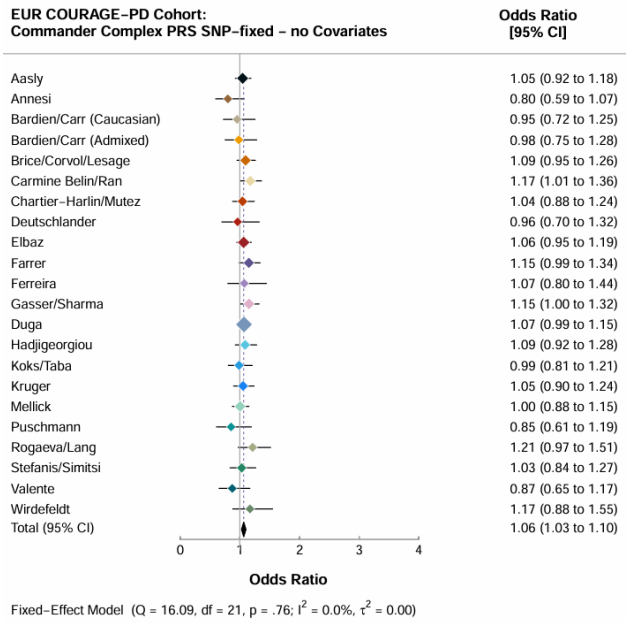

b.

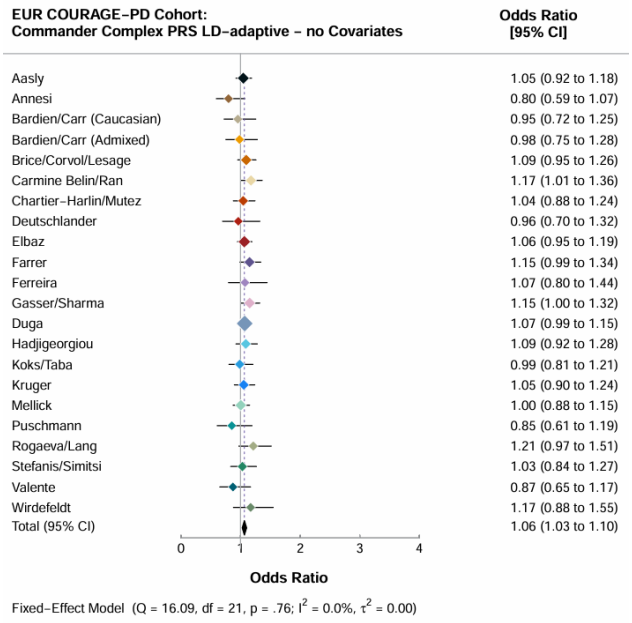

Supplementary Fig. 27: Random-Effect Meta-Analysis using SNPs overlapping the Commander Complex genes – no covariates

a.

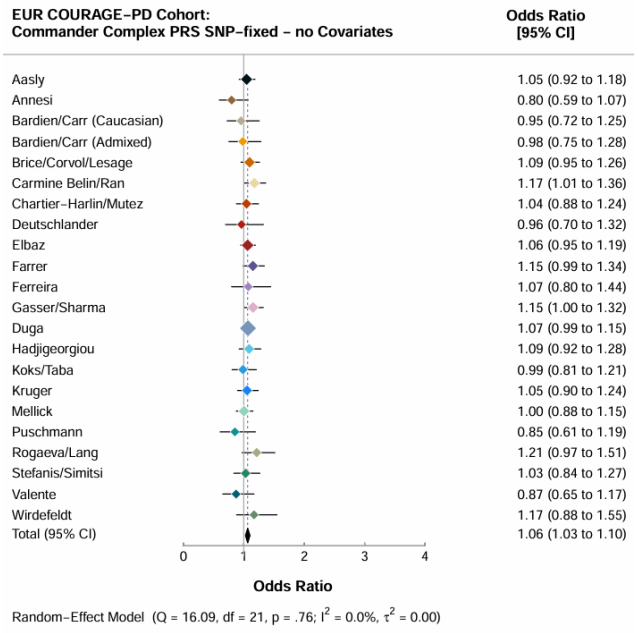

b.

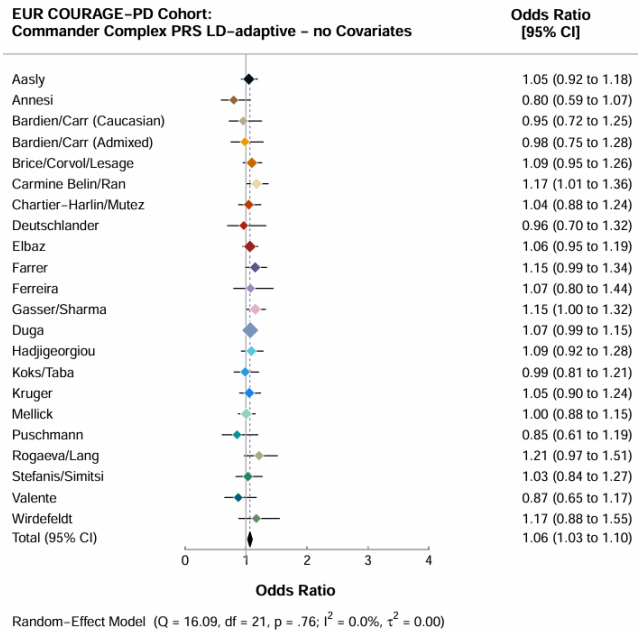

Supplementary Fig. 28: Cross-Dataset Heatmap of Cell-Type–Specific Differential Expression of PD Risk Genes

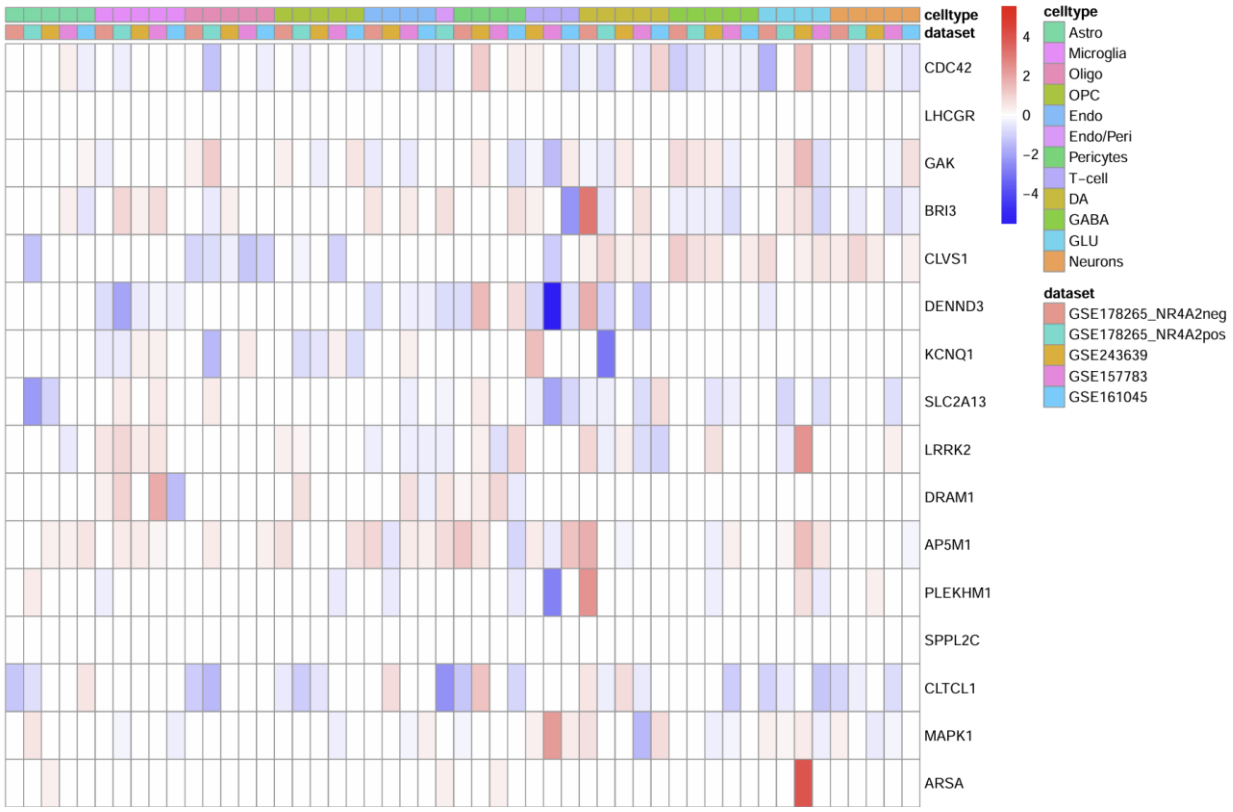

Heatmap depicting $\log_2$ fold-change ($\log_2$FC) of PD risk genes across cell types and datasets, calculated using Seurat *FindMarkers* (Wilcoxon test). Columns correspond to dataset–cell type combinations. Red indicates higher expression in PD, blue indicates lower expression, and white denotes comparisons that did not meet differential expression filtering criteria.

References

1. Kamath T, Abdulraouf A, Burris SJ, Langlieb J, Gazestani V, Nadaf NM, Balderrama K, Vanderburg C, Macosko EZ. Single-cell genomic profiling of human dopamine neurons identifies a population that selectively degenerates in Parkinson's disease. Nat Neurosci. 2022 May;25(5):588-595. doi: 10.1038/s41593-022-01061-1. Epub 2022 May 5. PMID: 35513515; PMCID: PMC9076534.

2. Martirosyan A, Ansari R, Pestana F, Hebestreit K, Gasparyan H, Aleksanyan R, Hnatova S, Poovathingal S, Marneffe C, Thal DR, Kottick A, Hanson-Smith VJ, Guelfi S, Plumbly W, Belgard TG, Metzakopian E, Holt MG. Unravelling cell type-specific responses to Parkinson's Disease at single cell resolution. Mol Neurodegener. 2024 Jan 20;19(1):7. doi: 10.1186/s13024-023-00699-0. Erratum in: Mol Neurodegener. 2024 Mar 25;19(1):28. doi: 10.1186/s13024-024-00717-9. PMID: 38245794; PMCID: PMC10799528.

3. Xu J, Farsad HL, Hou Y, Barclay K, Lopez BA, Yamada S, Saliu IO, Shi Y, Knight WC, Bateman RJ, Benzinger TLS, Yi JJ, Li Q, Wang T, Perlmutter JS, Morris JC, Zhao G. Human striatal glia differentially contribute to AD- and PD-specific neurodegeneration. Nat Aging. 2023 Mar;3(3):346-365. doi: 10.1038/s43587-023-00363-8. Epub 2023 Feb 9. PMID: 36993867; PMCID: PMC10046522.

4. Badanjak K, Mulica P, Smajic S, Delcambre S, Tranchevent LC, Diederich N, Rauen T, Schwamborn JC, Glaab E, Cowley SA, Antony PMA, Pereira SL, Venegas C, Grünewald A. iPSC-Derived Microglia as a Model to Study Inflammation in Idiopathic Parkinson's Disease. Front Cell Dev Biol. 2021 Nov 5;9:740758. doi: 10.3389/fcell.2021.740758. PMID: 34805149; PMCID: PMC8602578.

5. Smajić S, Prada-Medina CA, Landoulsi Z, Ghelfi J, Delcambre S, Dietrich C, Jarazo J, Henck J, Balachandran S, Pachchek S, Morris CM, Antony P, Timmermann B, Sauer S, Pereira SL, Schwamborn JC, May P, Grünewald A, Spielmann M. Single-cell sequencing of human midbrain reveals glial activation and a Parkinson-specific neuronal state. Brain. 2022 Apr 29;145(3):964-978. doi: 10.1093/brain/awab446. PMID: 34919646; PMCID: PMC9050543.

6. Aleknonytė-Resch M, Trinh J, Leonard H, Delcambre S, Leitão E, Lai D, Smajić S, Orr-Urtreger A, Thaler A, Blauwendraat C, Sharma A, Makarious MB, Kim JJ, Lake J, Rahmati P, Freitag-Wolf S, Seibler P, Foroud T, Singleton AB; International Parkinson Disease Genomics Consortium; Grünewald A, Kaiser F, Klein C, Krawczak M, Dempfle A. Genome-wide case-only analysis of gene-gene interactions with known Parkinson's disease risk variants reveals link between LRRK2 and SYT10. NPJ Parkinsons Dis. 2023 Jun 29;9(1):102. doi: 10.1038/s41531-023-00550-9. PMID: 37386035; PMCID: PMC10310744.

7. Hao Y, Stuart T, Kowalski MH, Choudhary S, Hoffman P, Hartman A, Srivastava A, Molla G, Madad S, Fernandez-Granda C, Satija R. Dictionary learning for integrative, multimodal and scalable single-cell analysis. Nat Biotechnol. 2024 Feb;42(2):293-304. doi: 10.1038/s41587-023-01767-y. Epub 2023 May 25. PMID: 37231261; PMCID: PMC10928517.

8. Wolock SL, Lopez R, Klein AM. Scrublet: Computational Identification of Cell Doublets in Single-Cell Transcriptomic Data. Cell Syst. 2019 Apr 24;8(4):281-291.e9. doi: 10.1016/j.cels.2018.11.005. Epub 2019 Apr 3. PMID: 30954476; PMCID: PMC6625319.

9. Korsunsky I, Millard N, Fan J, Slowikowski K, Zhang F, Wei K, Baglaenko Y, Brenner M, Loh PR, Raychaudhuri S. Fast, sensitive and accurate integration of single-cell data with Harmony. Nat Methods. 2019 Dec;16(12):1289-1296. doi: 10.1038/s41592-019-0619-0. Epub 2019 Nov 18. PMID: 31740819; PMCID: PMC6884693.